Regional Differences in South American Monsoon Precipitation Inferred from the Growth and Isotopic Composition of Tropical Trees*

A. P. Ballantyne[+,#] and P. A. Baker

Nicholas School of the Environment and Earth Sciences, Duke University, Durham, North Carolina

J. Q. Chambers

Climate Sciences Department, Lawrence Berkeley National Laboratory, Berkeley, California

R. Villalba

Instituto Argentina de Nivologia, Glaciologia y Ciencias Ambientales (IANIGLA), Mendoza, Argentina

J. Argollo

Instituto de Investigaciones Geológicas y del Medio Ambiente, Universidad Mayor de San Andrés, La Paz, Bolivia

Received 13 August 2008; accepted 25 September 2010

---

* Supplemental information related to this paper is available at the Journals Online Web site: http://dx.doi.org/10.1175/2010EI277.s1.

[+] Current affiliation: Geological Sciences Department, University of Colorado, Boulder, Colorado.

[#] Corresponding author address: A. P. Ballantyne, Geological Sciences Department, University of Colorado, Boulder, CO 80309-0399

E-mail address: ashley.ballantyne@colorado.edu

DOI: 10.1175/2010EI277.1

ABSTRACT: The authors present results on the relationship between tree-ring proxies and regional precipitation for several sites in tropical South America. The responsiveness of oxygen isotopes ($\delta^{18}O$) and seasonal growth as precipitation proxies was first validated by high-resolution sampling of a *Tachigali myrmecophila* from Manaus, Brazil (3.1°S, 60.0°W). Monthly growth of *Tachigali* spp. was significantly correlated with monthly precipitation. Intra-annual measurements of cellulose $\delta^{18}O$ in *Tachigali* spp. were also significantly correlated with monthly precipitation at a lag of approximately one month. The annual ring widths of two tropical tree taxa, *Cedrela odorata* growing in the Amazon (12.6°S, 69.2°W) and *Polylepis tarapacana* growing in the Altiplano (22.0°S, 66.0°W), were validated using bomb-derived radiocarbon ^{14}C. Estimated dates were within two to three years of bomb-inferred ^{14}C dates, indicating that these species exhibit annual rings but uncertainties in our chronologies remain. A multiproxy record spanning 180 years from *Cedrela* spp. showed a significant negative relationship between cellulose $\delta^{18}O$ and January precipitation. A 150-yr record obtained from *Polylepis* spp. also showed a significant negative relationship between $\delta^{18}O$ and March precipitation, whereas annual ring width showed a significant positive correlation with December precipitation. These proxies were combined in a multivariate framework to reconstruct past precipitation, revealing a significant increase in monsoon precipitation at the Amazon site since 1890 and a significant decrease in monsoon precipitation at the Altiplano since 1880. Proxy time series also showed spatial and temporal coherence with precipitation variability due to El Niño forcing, suggesting that oxygen isotopes and ring widths in tropical trees may be important diagnostics for identifying regional differences in the response of the tropical hydrologic cycle to anthropogenic warming.

KEYWORDS: Stable isotopes; Tropical trees; Global change

1. Introduction

The short duration and scarcity of instrumental climate records from the tropics makes our knowledge of tropical climate variability over the last century very limited (Trenberth et al. 2007). Thus, paleoclimate records from the tropics are critical for evaluating background climate variability and for documenting the response of tropical latitudes to anthropogenic climatic forcing over the twentieth century (Evans and Schrag 2004). A great deal has been learned about changes in tropical sea surface temperatures (SSTs) and their response to El Niño–Southern Oscillation (ENSO) variability from the geochemical composition of modern corals. Although these records suggest an increase in ENSO frequency (Urban et al. 2000) in response to warmer SSTs, periods of heightened ENSO frequency have also been documented for discrete periods in Earth's past by examining fossil corals (Tudhope et al. 2001). Because ENSO is so important in modulating tropical precipitation, it would be useful to have a similar network of annually resolved climate records from the terrestrial tropics to evaluate the spatial and temporal response of precipitation to ENSO variability. Unfortunately, similar high-resolution proxy records from the terrestrial tropics are scarce.

Northern Hemisphere climate reconstructions of the past 1000 years are heavily reliant on annual ring-width measurements in trees growing at high latitudes, where ring width is primarily a function of mean annual temperature or mean growth season temperature (Jones and Mann 2004). However, very few studies have employed dendrochronological techniques to reconstruct tropical climate variability. This is

mainly due to the a priori assumption that tropical tree species do not have annual growth rings. Although there are many tropical trees that do not exhibit annual growth rings, several tropical tree taxa growing in a wide variety of tropical settings have been identified with annual growth rings. Several studies have identified tropical trees with annual growth rings in tropical South America (Dunisch et al. 2003; Worbes 1999), Central America (Enquist and Leffler 2001), and Southeast Asia (Buckley et al. 2007; D'Arrigo et al. 2006), suggesting that certain tree taxa in certain tropical forests may respond to seasonal climate variability by forming annual rings.

In fact, most tropical locations experience limited variation in seasonal temperatures, but experience pronounced variations in seasonal precipitation. Within the tropics as much as 80% of the forest is characterized as seasonally "dry forest" (Murphy and Lugo 1986), thus differential growth rates in response to the seasonal availability of water should be manifested as changes in the wood anatomy of many tropical trees. Furthermore, most of the previous studies documenting annual growth rings in tropical trees have reported a significant relationship between annual growth and seasonal precipitation (Worbes 1999) or drought (Buckley et al. 2007; D'Arrigo et al. 2006) and in some instances precipitation occurring in the previous year (see Enquist and Leffler 2001; Dunisch et al. 2003). These correlations between seasonal precipitation and annual ring widths at low latitudes ($0.2 < r < 0.6$) are comparable to those of other proxies conventionally used to reconstruct temperature at high latitudes ($0.2 < r < 0.8$; Jones and Mann 2004), although they are slightly weaker than the relationship between and annual ring widths and drought in the western United States ($0.5 < r < 0.7$; Cook et al. 2004). Therefore, annual growth rings in some tropical tree taxa growing in the right setting may be an effective proxy of precipitation variability and may provide valuable climate insight at tropical latitudes where instrumental data are sparse.

In addition to ring-width chronologies, several recent studies have explored stable isotopes in tropical trees as an independent proxy of tropical precipitation variability. This approach is based upon the observation that the hydrogen and oxygen isotopic composition of precipitation in most of the tropics is well correlated with precipitation amount (Dansgaard 1964; Rozanski et al. 1993). Therefore, if tropical trees assimilate rainwater into cellulose in a systematic fashion, then it should be possible to relate the isotopic composition of cellulose to past changes in the amount of precipitation (Evans and Schrag 2004). A previous study attempting to characterize the Asian monsoon using hydrogen isotopic ratios in cellulose was variably successful (Ramesh et al. 1989) but ultimately had trouble reconciling the competing effects of temperature and precipitation on isotopic variability. A high-amplitude signal of 9‰ in the oxygen isotopes of trees growing in Costa Rica has been identified, suggesting high fidelity in tropical trees at recording the isotopic signature of seasonal precipitation variability (Anchukaitis et al. 2008b; Evans and Schrag 2004). Similar seasonal variability has been observed in the oxygen and carbon isotopes from both *Quercus kerrii* and *Miliusa velutina* growing in Thailand (Poussart and Schrag 2005). Although, changes in the isotopic amplitude in these species were indicative of a decrease in monsoon precipitation over time, the length of the isotopic record (~50 years) precluded the possibility of reconstructing precipitation prior to the instrumental record (Poussart and Schrag 2005). Similarly, poorly constrained radiometric dates in many studies of isotopes in tropical trees lacking annual growth rings (Evans and Schrag 2004; Poussart and

Schrag 2005) have made it exceedingly difficult to make inferences about changes in precipitation variability on annual time scales.

Our objective in this study was to develop a multiproxy approach to reconstructing precipitation variability based on the simultaneous measurement of annual ring width and isotopic variability in trees from tropical South America. Our hypothesis that growth and isotopic variability in tropical trees are sensitive to seasonal precipitation was first tested on an Amazonian taxon for which monthly growth and precipitation data were available. We then analyzed the temporal relationship between local precipitation and annual growth rings as well as carbon and oxygen isotopes in other longer-lived tropical tree taxa. Finally, multivariate models combining proxy information were developed to hindcast regional monsoon precipitation over the instrumental record and ultimately reconstruct precipitation variability prior to the instrumental record.

2. Theoretical approach

2.1. Dendrochronological approach in the tropics

Numerous studies have identified annual growth rings in tropical trees (Buckley et al. 2007; D'Arrigo et al. 2006; Dunisch et al. 2003; Enquist and Leffler 2001; Morales et al. 2004; Solíz et al. 2009; Villalba et al. 1992; Worbes 1999), and several of these studies have reported significant relationships between annual growth and seasonal precipitation (Dunisch et al. 2003; Solíz et al. 2009; Villalba et al. 1998). In two of the three sites investigated in this study, we focused our sampling efforts on tree taxa that are known to form annual rings that are sensitive to seasonal precipitation. For our study of climate variability in tropical South America, we focused on *Cedrela odorata* and *Polylepis tarapacana*, both of which are known to have annual rings that are sensitive to the amount of seasonal precipitation (Dunisch et al. 2003; Solíz et al. 2009; Villalba et al. 1992). We also investigated *Tachigali myrmecophila* growing in the central Amazon. Although *Tachigali myrmecophila* does not appear to have growth rings, monthly growth rates and tree cores were available for the individual included in this study.

2.2. Isotopic theory and application

Carbon isotopes in plant cellulose provide an integrated proxy of water lost and carbon gained during photosynthesis. The isotopic discrimination of carbon ($\Delta^{13}C$) during photosynthesis is best described by the following mechanistic model (Farquhar et al. 1989):

$$\Delta^{13}C = a + c_i/c_a(b - a) + \varepsilon_{cx}, \tag{1}$$

where

$$\Delta^{13}C = \frac{\delta^{13}C_{atm} - \delta^{13}C_{cx}}{1 + \delta^{13}C_{cx}}. \tag{2}$$

Thus, the isotopic ratio of cellulose ($\delta^{13}C_{cx}$) varies as a function of changes in isotopic composition of atmospheric CO_2 ($\delta^{13}C_{atm}$; Francey et al. 1999) fractionated

by the diffusion of atmospheric CO_2 into the leaf ($a = 4.4‰$), the net carboxylation by rubisco ($b = -27.7‰$), the partial pressures of intercellular CO_2 (c_i), the partial pressure of atmospheric CO_2 (c_a), and the enrichment of sucrose when it is converted to cellulose ($\varepsilon_{cx} = 3.5‰$). It is evident from this formulation that values of $\delta^{13}C_{cx}$ vary as a function of source $\delta^{13}C_{atm}$ and c_i/c_a, which is regulated by stomatal conductance. Although stomatal conductance can vary because of factors affecting assimilation and transpiration, here we use $\Delta^{13}C$ as an integrated proxy of stomatal conductance (Farquhar et al. 1989). Therefore, under drought conditions, we would predict a reduction in stomatal conductance, indicated by a diminished c_i/c_a, and ultimately a decrease in $\Delta^{13}C$.

Similar models describing oxygen isotopes in plants have been developed (Roden et al. 2000) where the isotopic ratio of oxygen in cellulose ($\delta^{18}O_{cx}$) is an admixture of the meteoric source water ($\delta^{18}O_{sw}$) and leaf water ($\delta^{18}O_{lw}$) that is isotopically enriched during transpiration:

$$\delta^{18}O_{cx} = f_o \times (\delta^{18}O_{sw} + \varepsilon_o) + (1 - f_o) \times (\delta^{18}O_{lw} + \varepsilon_o), \tag{3}$$

where f_o is the proportion of the carbon-bound oxygen that exchanges with source water. This fraction f_o of 0.42 has been determined from a several broad-leaf trees growing at varying levels of humidity. The $\delta^{18}O_{cx}$ is enriched ($\varepsilon_o = 27‰$) with respect to leaf water because of the carbonyl–water interaction during biosynthesis (Sternberg and Deniro 1983). The isotopic enrichment of leaf water is a complex physical process primarily controlled by the kinetic fractionation due to temperature (Majoube 1971). In theory, however, the isotopic enrichment of leaf water should be greatly reduced in tropical forests because of increased relative humidity, and thus $\delta^{18}O_{cx}$ should reflect a greater proportion of $\delta^{18}O_{sw}$ (Evans and Schrag 2004), which varies as a function of precipitation amount at tropical latitudes (Bowen 2008).

2.3. Multivariate statistical approach

The models describing the physical processes underlying isotopic fractionation in cellulose [Equations (1) and (3)] and empirical relationships between tree growth and environmental factors allow us to combine proxy information in a multivariate statistical framework to make inferences about climate variability. Although there are assumptions and errors associated with each of our proxy measurements, the physical processes controlling growth and isotopic fractionation are ultimately governed by climate. Thus, we have devised the following multivariate framework to evaluate the amount of variance in the underlying climate process explained by our proxy measurements:

$$P = \beta_o + \beta_1\chi_1 + \beta_2\chi_2 + \beta_3\chi_3 \cdots \beta_n\chi_n + \varepsilon. \tag{4}$$

In this case, the underlying climate process is seasonal precipitation (P) and the model parameters include the intercept (β_o) and the slope terms ($\beta_1, \ldots, \beta_n$) for each respective proxy ($\chi_1, \ldots, \chi_n$), as well as an error term (ε). Such a multivariate framework is very flexible and allows one to combine proxy data to capture the variability of any climate process. This model was optimized at each site by evaluating the effectiveness of our proxies (i.e., ring width, $\delta^{13}C_{cx}$, and $\delta^{18}O_{cx}$) at

capturing precipitation variability. The effectiveness of individual proxies at capturing precipitation variability was first evaluated by examining changes in the Pearson's correlation (r) for each month. Then proxies were combined in the multivariate framework [Equation (4)] to hindcast seasonal observations of precipitation at each site and optimal models were selected based on maximum r and p values, as well as minimum values of Akaike's information criterion (AIC). Cross-validation statistics (X_{val}) were also calculated based on the removal of random samples in 10 groups to derive new estimates of fitted model predictions that were then correlated with actual precipitation data. The optimal model for each site was then used to predict regional patterns of precipitation variability and reconstruct past precipitation variability at each site prior to the instrumental record.

All regression models among variables at each site and spatial correlations were performed using the fields package in *R* (Nychka 2007). The shared variance between all proxy data was estimated using a principal components analysis. Principal components scores were then compared to the spatial variability of seasonal precipitation and the temporal variability associated with ENSO. Finally, proxy time series were analyzed in the frequency domain by applying the Morlet wavelet and comparing changes in frequency to dominant ENSO frequencies using the coherence wavelet transform function of Grinsted et al. (Grinsted et al. 2004).

3. Analytical methods and site descriptions

3.1. Selection and description of tropical sites

For this study, we selected three sites spanning a precipitation and altitudinal gradient across tropical South America (Figure 1). Our first site was Manaus, Brazil (3.1°S, 60.0°W, 72 m MSL), in the central Amazon, which has a mean annual temperature of 27.6°C and a total annual precipitation of 2.20 m. Approximately half of the precipitation at Manaus occurs from December to March (DJFM), and the dry season, in which monthly precipitation does not exceed 100 mm, extends from July to August. The second location selected for sampling was Puerto Maldonado, Peru (12.6°S, 69.2°W, 265 m MSL), located in the western Amazon, where mean annual temperature is 24.2°C and total annual precipitation is 2.40 m. The dry season in Puerto Maldonado extends from May to August, with 47% of precipitation occurring between December and February. Finally, samples were collected from Volcan Granada (22.0°S, 66.0°W, 3500 m MSL) in northern Argentina, where mean annual temperature is 8.7°C and total annual precipitation is 0.48 m, with 70% occurring between December and February and precipitation not exceeding 100 mm in any month of the year. Although these sites represent a range of climatological regimes and biomes within the tropics, all sites experience seasonal variability in precipitation.

3.2. Tropical tree species sampled

In this study, we focused on three different dominant species at each of these sites. First, we selected a single individual of the fast-growing species, *Tachigali myrmecophila*, from Manaus, Brazil. *T. myrmecophila* is a shade-tolerant emergent tree with long-lived leaves and no apparent annual growth rings (Fonseca and Benson 2003). The circumferential growth of trees at this site has been measured

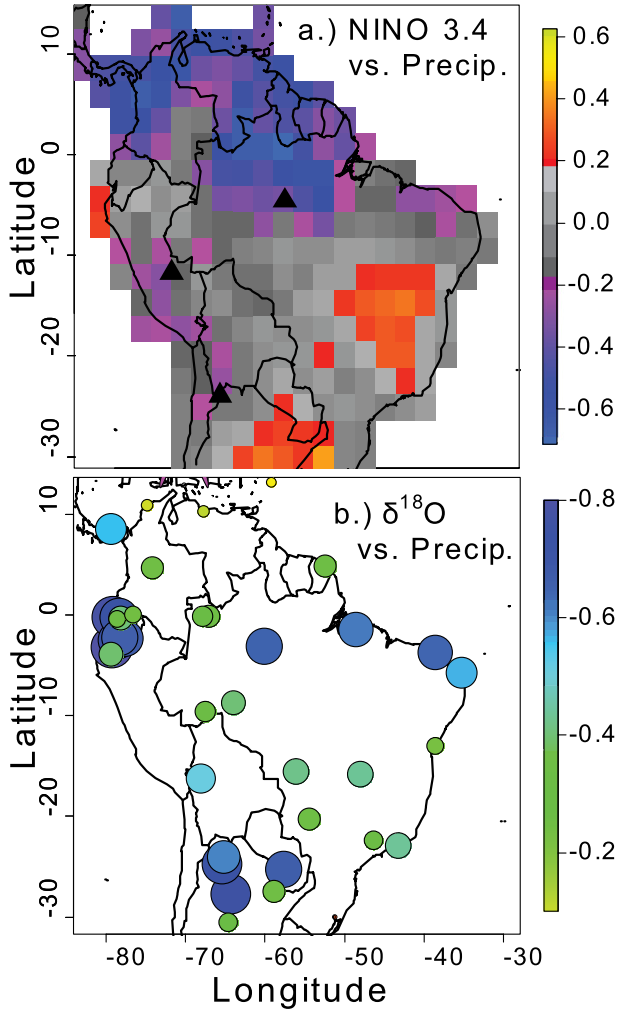

Figure 1. Relationship between the amount of rainy season precipitation, El Niño variability, and oxygen isotopes in precipitation. (a) Plotted are the correlation coefficients (r) between precipitation (Dai et al. 1997) and Niño-3.4 for JFM from 1857 to 2004 ($N = 147$). Tree core sampling locations are plotted as filled triangles. Regions where El Niño events are associated with significant changes in precipitation (p value < 0.05; $-0.17 < r < 0.17$) are plotted in color. (b) Plotted are the correlation coefficients (r) between monthly values of oxygen isotopes ($\delta^{18}O$ ‰ SMOW) and precipitation amount, from 38 IAEA stations (IAEA/WMO 2004) located in tropical South America (see Table S1 for statistics and information on each site).

almost every month since June 1999, allowing for seasonal growth resolution. Circumferential growth was measured using an in situ dendrometer band located at 1.3-m height above any buttresses and digital calipers with a precision of 10 μm. Growth measurements were taken throughout the day, so small daily changes in stem circumference from transpiration-induced stem contraction did not introduce

any bias (da Silva et al. 2002). A core sample was extracted from one of these individuals in May 2003.

Several species of tropical trees with reported annual rings were sampled from a logging operation near Puerto Maldonado, Peru. Two radial cross sections were cut from felled logs for each species. These radial cross sections were then examined in the laboratory, and a sample of *Cedrela odorata* was selected based on the clarity of ring boundaries and the approximate length of the record (184 years). Ring widths were measured in both radii using a video camera mounted to a dissecting scope interfaced with a positioning table. *Cedrela* is a widespread midsuccessional tree that grows slowly until emerging from the forest canopy (Terborgh et al. 1997).

Finally, we sampled *Polylepis tarapacana*, the tree species with the highest altitudinal range in the world, from Volcan Granada, Argentina. *Polylepis* is a slow-growing tree with annual growth rings known to be sensitive to seasonal precipitation (Morales et al. 2004). This individual tree was selected from a larger population of *Polylepis* used to generate a regional ring-width chronology (Solíz et al. 2009). This subpopulation from Volcan Granada included 47 radii from 26 trees with a mean ring width of 0.848 mm. Cores from this subpopulation were cross-dated using the COFECHA program (Holmes 1983), and standardized ring-width chronologies were generated and evaluated using standard dendrochronological techniques in the TURBO ARSTAN program (Cook and Holmes 1984). The subpopulation from Volcan Granada had 0.017% missing rings with a mean sensitivity of 0.368 and 35.62% of the variance explained by the first eigenvector, as well as an Rbar value of 0.339 $\pm$ 0.007 (Solíz et al. 2009), suggesting that ring widths in this subpopulation are annual and are responding coherently to regional climate variability. The residual ring-width chronology included in our analysis is from the Volcan Granada subpopulation. From this subpopulation, we selected one long-lived individual for our isotopic analysis that was highly correlated with the regional climate reconstruction ($R^2 = 0.90$), suggesting that this individual was representative of the larger population. Unfortunately, because of the thin annual growth bands in *Polylepis,* there was only enough material for $\delta^{18}O_{cx}$ analysis and not $\delta^{13}C_{cx}$.

The single *Tachigali* sample from Manaus was thinly sliced (~200-μm thickness) using a microtome. Thin sections were then placed into microcentrifuge vials for cellulose extraction. Cross sections from *Cedrela* and *Polylepis* were sanded and polished to highlight the boundaries between annual rings. Two radii of *Cedrela* and *Polylepis* were subsampled using a micromill (Merchantek, California) equipped with a 0.5-mm diamond bit (Dremel). Sample trajectories were overlaid on the sample using imaging software (Merchantek EO, California), and the rotational speed of the drill was reduced to avoid burning of wood that may result in isotopic fractionation. The pulverized samples were collected with a dental probe and placed in microcentrifuge tubes for cellulose extraction. Sample trajectories were cleaned using compressed air to prevent contamination between samples of annual rings.

3.3. Cellulose extraction and isotopic analysis

Recent advances in organic chemistry and mass spectrometry have greatly expedited rates of cellulose extraction and increased throughput of isotopic analyses. Isotopic analysis has previously been performed on whole wood samples; however,

this results in the loss of isotopic variability potentially attributable to climatic variables and thus extraction of α cellulose has been suggested (Borella et al. 1999). For this study, we used a modified Brendel method for small samples (Evans and Schrag 2004). Although the Brendel method may lead to trace levels of contamination that may hinder ^{14}C methods of dating α cellulose (Gaudinski et al. 2005), it has been shown that $\delta^{18}O_{cx}$ measurements made on α cellulose extracted using this method are statistically indistinguishable from α cellulose extracted using conventional methods (Anchukaitis et al. 2008a). Ground samples of cellulose were acidified and heated to remove lignin followed by a series of rinsing and centrifuging steps. Samples were then dried in an oven at 60°C for 24 h and stored in an anoxic dessicator. Dry subsamples were individually weighed and encapsulated in silver capsules for the analysis of oxygen and in tin capsules for the analysis of carbon isotopes. To compare our ring-width chronology with the atmospheric ^{14}C peak associated with nuclear weapons testing, a subset of cellulose samples were further rinsed using a 17% NaOH solution, which has been shown to reduce contamination (Gaudinski et al. 2005); dried; and analyzed for ^{14}C [Center for Accelerator Mass Spectrometry (CAMS), Lawrence Livermore National Laboratory]. Cellulose was also extracted from a sample of ^{14}C dead wood (Queets abrnd) as an internal standard in our analysis. Because our sites are located in the Southern Hemisphere tropics, our ^{14}C measurements were compared with the continuous atmospheric ^{14}C curve from Wellington, New Zealand (41°S, 174°E; Manning and Melhuish 1994), and two discontinuous ^{14}C curves from Debre Zeit, Ethiopia (8°N, 38°E), and Fianarantsoa, Madagascar (21°S, 47°E; Nydal and Lövseth 1983).

Oxygen and carbon isotopes were measured using continuous flow mass spectrometry. Homogenized cellulose samples were thermally converted in the absence of oxygen (Finnigan MAT TC/EA) and then analyzed for $\delta^{18}O$ by mass spectrometry (Finnigan MAT Delta plus XL). For $\delta^{13}C$ determination, cellulose samples were combusted in a Carlo Erba elemental analyzer, prior to analysis on the same mass spectrometer. Average instrumental precision was $\pm 0.2‰$ for oxygen isotopes and $\pm 0.1‰$ for carbon isotopes, based on the offset in measurements from a barium sulfate standard of known oxygen isotopic composition [NBS 127] and a mineral oil standard of known carbon isotopic composition [NBS 22], as well as a working cellulose that were included with every series of analyses. The reference gases used were National Specialty Gases laser grade CO_2 with a purity of 99.995% and $-44.0‰$ $\delta^{13}C$ [Pee Dee Belemnite (PDB)] and Messer Greisheim CO with a purity of 99.997% and $-5.5 \pm 2.0‰$ $\delta^{18}O$ [Standard Mean Ocean Water (SMOW)]. According to convention, stable isotopes of carbon and oxygen are expressed as a ratio between the heavier and the lighter isotopes in a sample (R) with respect to the ratio of isotopes in an arbitrary standard (R_{st}) and conventionally reported as $\delta = [(R - R_{st})/R_{st}] \times 1000$. Isotopic ratios of oxygen ($\delta^{18}O$) are reported with respect to Vienna SMOW (V-SMOW; $R_{st} = 2.0052 \times 10^{-3}$), and isotopic ratios of carbon ($\delta^{13}C$) are reported with respect to PDB ($R_{st} = 1.123\,72 \times 10^{-2}$).

3.4. Data acquisition and processing

To identify regions where precipitation and $\delta^{18}O$ are strongly correlated, we compiled sites from International Atomic Energy Administration's network located in tropical South America (IAEA/WMO 2004). Sites with at least two years

of observations of $\delta^{18}O$ and precipitation amount were included in our correlation analysis (online supplement Table S1). The response in spatial variability of seasonal precipitation to variability in ENSO was also analyzed to identify potentially suitable regions for reconstructing precipitation variability sensitive to ENSO forcing. For this analysis, we used the sea surface temperature anomaly index Niño-3.4 obtained from the National Center for Atmospheric Research and defined by Trenberth (Trenberth 1997). For our site-specific analyses of the relationship between tree-ring proxies and monthly precipitation, we acquired precipitation data from the recently updated global database of observed precipitation from Dai et al. (Dai et al. 1997). Because instrumental precipitation data are so sparse and often discontinuous in this region, we calculated the mean of the four grid cells encompassing our field sites for comparison with our proxy data.

4. Results

4.1. Spatial patterns of ENSO, precipitation, and oxygen isotopes

The anomalous SSTs associated with positive and negative phases of ENSO exert a large control on interannual variation of precipitation throughout much of the tropics (Lyon 2004), including tropical South America (Vuille and Werner 2005). El Niño events generally result in increased precipitation during the summer months of January–March (JFM) in coastal Ecuador, northern Argentina, and the Bahia region of Brazil and decreased JFM precipitation in much of the equatorial Amazon basin. Regions that experience the most significant reductions in precipitation in response to ENSO events include central Brazil, Venezuela, and coastal Colombia, as well as the Peruvian Amazon and the Altiplano of Peru (Figure 1a), which is broadly consistent with previous analyses (Malhi and Wright 2004). However, extreme precipitation events in the Amazon also occur independently of ENSO. For example, the historic Amazonian drought of 2005 was caused by anomalously warm SSTs in the northern tropical Atlantic, as well as reduced northeast trade winds and convection over the basin (Marengo et al. 2008).

Our analysis verified the significant inverse relationship between the oxygen isotopic composition of precipitation and precipitation amount over most of tropical South America (Figure 1b and Table S1), albeit with considerable spatial variability. This relationship is quite strong between 30°S and 30°N, with the exception of sites along the Caribbean coast in Colombia and Venezuela that showed only moderate correlation. Regions where the relationship between $\delta^{18}O_{sw}$ and precipitation amount are highly significant are sites in Ecuador [Uzchurrimi: $r = -0.715$, p value $= 0.0006$, and degrees of freedom (DF) $= 32$; Cuenca: $r = -0.662$, p value $= 0.0008$, and DF $= 23$], Manaus, Brazil ($r = -0.61$, p value $= 0.0016$, DF $= 186$); and Salta, Argentina ($r = -0.67$, p value $= 0.0006$, DF $= 42$). However, this relationship is greatly diminished beyond the tropical latitudes of Argentina and Mexico. Despite the strong precipitation gradient between our study sites in the lowland Amazon forest and the Andes, there is a persistent inverse relationship between $\delta^{18}O_{sw}$ and precipitation amount and precipitation amount is sensitive to ENSO variability across all sites (Figure 1). This suggests that these sites are suitable for evaluating the relationship between $^{18}O_{cx}$ and seasonal precipitation, as well as the sensitivity of seasonal precipitation to fluctuations in ENSO.

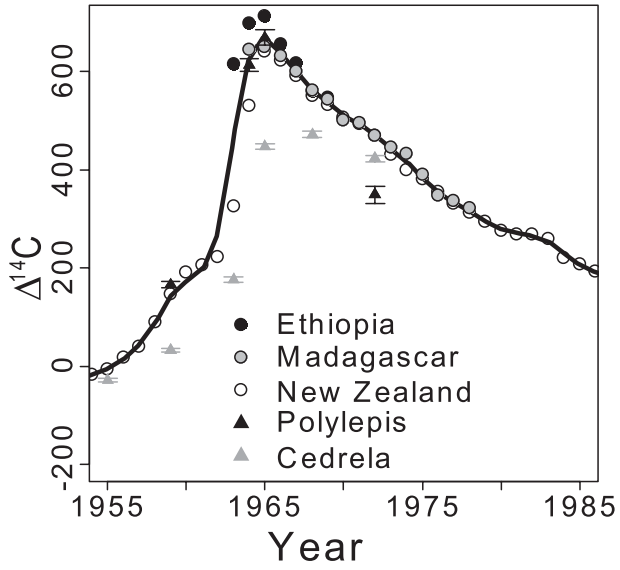

Figure 2. Content of the radiogenic carbon isotopes ($\Delta^{14}C$) in annual rings of tropical trees compared with atmospheric ^{14}C measured at three locations. The $\Delta^{14}C$ content of cellulose samples from *Polylepis tarapacana* (black triangles) and *Cedrela odorata* (gray triangles) are plotted with error bars (standard error (SE±)). Annual average values of $\Delta^{14}C$ content of atmospheric CO_2 measured at Debre Zeit, Ethiopia (8°N, 38°E), and Fianarantsoa, Madagascar (21°S, 47°E), from Nydal and Lövseth (Nydal and Lövseth 1983) and at Wellington, New Zealand (41°S,174°E), from Manning and Melhuish (Manning and Melhuish 1994). A spline function has been fit to the atmospheric data and this spline function was used for correlating atmospheric $\Delta^{14}C$ measurements with our $\Delta^{14}C$ tree-ring measurements.

4.2. Chronology and seasonal isotopic variability

There is a clear relationship between radiogenic carbon ($\Delta^{14}C$) measured within the cellulose of the trees investigated and the atmospheric peak in bomb $\Delta^{14}C$, but with some key differences between $\Delta^{14}C$ measurements in each species (Figure 2). There is a strongly significant statistical relationship between atmospheric $\Delta^{14}C$ and the $\Delta^{14}C$ values measured in the cellulose of growth rings in both species ($R^2 = 0.90$; p value $= 0.002$, $N = 10$, and DF $= 8$), suggesting that the growth rings observed in these trees are not random. However, our cellulose $\Delta^{14}C$ values tend to be biased low relative to the atmosphere, especially in *Cedrela*. Values of $\Delta^{14}C$ in *Polylepis* correspond well with bomb-derived $\Delta^{14}C$ measured in the Southern and Northern Hemispheres (RMSE ± 2.0 yr). The correspondence between $\Delta^{14}C$ values in *Polylepis* and $\Delta^{14}C$ in the atmosphere in conjunction with statistics showing very few missing rings and a coherent climate signal among the subpopulation of trees from which this tree was subsampled (see section 3.2) provides strong independent lines of evidence that rings in *Polylepis* are formed annually. In contrast, although values of $\Delta^{14}C$ in *Cedrela* reflect the general distribution

of $\Delta^{14}C$ in the atmosphere (RMSE ± 2.4 yr), they are consistently depleted by 10‰–200‰. This systematic bias in $\Delta^{14}C$ could potentially lead to an error in our *Cedrela* chronology. The greatly attenuated $\Delta^{14}C$ peak apparent in *Cedrela* could be due to contamination during our analysis or an unexplained source of atmospheric CO_2 predating the bomb-derived ^{14}C. Trace amounts of modern ^{14}C (mean fraction modern = 0.0003) were measured in our internal standard of ^{14}C dead wood, indicating that as much as 10 μg of contaminated carbon was introduced during cellulose extraction. However, cellulose was extracted from both *Cedrela* and *Polylepis* using the exact same protocol, and yet there is very little evidence of contamination in three of the four *Polylepis* samples. Previous studies of annual chronologies derived from both *Cedrela* growing in the Amazon (Dunisch et al. 2003) and northern Argentina (Villalba et al. 1992), as well as *Polylepis* growing in northern Argentina (Morales et al. 2004) and the Altiplano of Bolivia (Solíz et al. 2009), suggest that these tropical tree taxa do exhibit annual growth rings. Although we have greater certainty in the chronological constraints of our *Polylepis* sample based on the ^{14}C dates and the cross-dating with other *Polylepis* samples from the region, we are less certain of the chronological constraints on our *Cedrela* because of the uncertainty in our ^{14}C measurements and the lack of cross-dating.

Seasonal changes in growth rate and $\delta^{18}O_{cx}$ of *Tachigali myrmecophila* growing in Manaus were remarkably coherent with seasonal changes in precipitation amount (Figure 3). A significant correlation was observed between monthly growth rate and precipitation ($r = 0.51$, p value = 0.0007, DF = 47, and AIC = 127.9). In contrast, there was no direct statistical relationship between $\delta^{18}O_{cx}$ and precipitation. However, if we allow the $\delta^{18}O_{cx}$ time series to lag precipitation by one month, then a significant statistical relationship emerges ($r = -0.43$, p value = 0.004, DF = 41, and AIC = 131.2), suggesting that minima in $\delta^{18}O_{cx}$ lag maxima in precipitation amount by approximately one month. These results are consistent with theory as growth increases in response to increased precipitation and $\delta^{18}O_{cx}$ decreases in response to increased precipitation. If we combine our proxies of growth rate and $\delta^{18}O_{cx}$ into a single multivariate model predicting precipitation, the correlation is improved ($r = 0.59$, p value = 0.0003, DF = 40, and AIC = 124.9). The increased r and p values in combination with the decreased AIC indicate that combining these proxies into a single multivariate model is more effective at predicting seasonal variability in precipitation than relying on either of these proxies independently. Although these results are not definitive because our measurements of $\delta^{18}O_{cx}$, growth, and monthly precipitation were not taken at the same time, they do provide compelling evidence for a relationship between precipitation amount and $\delta^{18}O_{cx}$ that is recorded in tropical trees as they grow.

4.3. Temporal variability in isotopes and ring widths and their relation to precipitation

The relatively large ring widths present in *Cedrela odorata* samples collected from the Peruvian Amazon allowed for the measurement of both oxygen and carbon isotopes revealing several significant relationships among tree-ring proxies (Table 1 and Figure 4). Ring widths measured in two radii from the same *Cedrela* were significantly correlated, suggesting that growth rings can be identified and

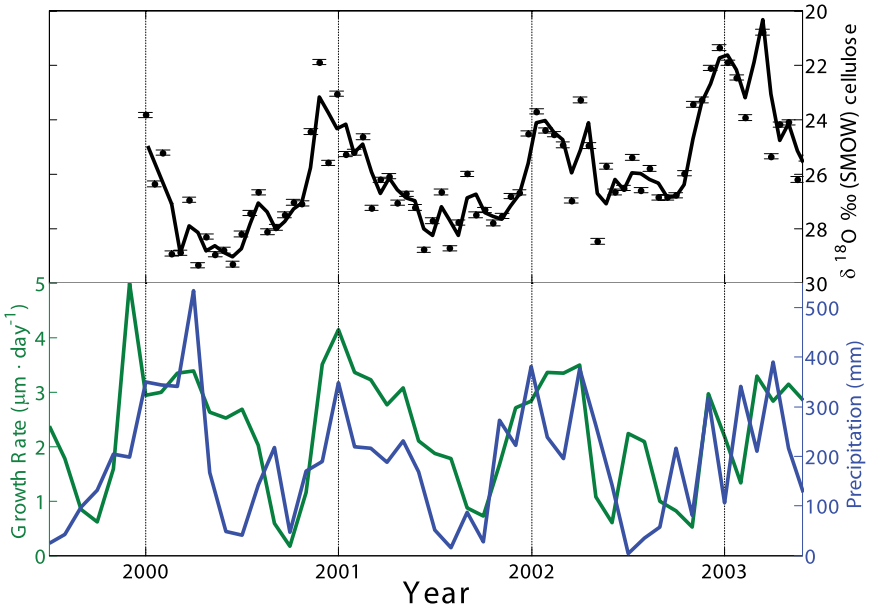

Figure 3. Growth rate and oxygen isotopic composition of *Tachigali myrmecophila* tree growing in Manaus, Brazil, compared with monthly precipitation. Cellulose $\delta^{18}O$ ‰ values (black circles) are plotted with error bars representing instrumental error and a 2-point moving average (black line). Plotted for comparison are in situ monthly growth measurements for *Tachigali myrmecophila* (green line) and monthly precipitation values (blue line) from Manaus, Brazil (data from updated global precipitation database of Dai et al. 1997).

measured in this taxa and that rings are circumferentially continuous (Table 1). Similarly, $\delta^{18}O_{cx}$ measured in two separate radii were significantly correlated, indicating that oxygen isotopes are being consistently incorporated and assimilated into the annual growth bands of this tree. The strongest relationship to emerge from this analysis was the significantly positive relationship between $\Delta^{13}C$ and annual ring width (Table 1), such that increased discrimination was associated with suppressed growth during early development (from AD 1830 to 1870; Figure 4). This period of suppressed growth, as evidenced by reduced ring width, also coincided with decreased interannual variability in the $\delta^{18}O_{cx}$ signal. Although only one of our time series of $\delta^{18}O_{cx}$ showed a marginally significant correlation with the Andean ice core index (AII), there was a significant negative correlation between one of our ring-width time series and the isotopic record from the AII (in Table 1 and Figure 4). However, the fact that this relationship was not evident in the second radii suggests that much of this signal is probably noise and the relationship between ring width and the AII would have to be verified with a regional ring-width chronology including multiple trees.

Our measurements of annual ring-width and isotopic variability in the individual *Polylepis* sampled from northern Argentina revealed significant relationships between $\delta^{18}O_{cx}$ values from two independent radii collected from the same tree

Table 1. Correlation matrix among proxies measured in two radii of *Cedrela odorata*, as well as previously published ice core $\delta^{18}O$ records. Pearson's correlation coefficients (*r*) are reported between parameters. Characteristics from *Cedrela odorata* (*N* = 184) are compared with $\delta^{18}O$ from the Quelccaya ice core (*N* = 160; Thompson et al. 1986) and the AII (*N* = 90; from Hoffmann et al. 2003). Ring widths and oxygen isotopes are reported for two different radii in the same tree (subscripts a and b), whereas carbon isotope data are reported for a single radius (a).

	Ring $width_a$	Ring $width_b$	$\Delta^{13}C_a$	$\delta^{18}O_a$	$\delta^{18}O_b$	Quelccaya	AII
Ring $width_a$		0.779***	−0.639***	0.112	0.001	−0.142	−0.221**
Ring $width_b$			0.125	−0.001	0.039	−0.120	−0.055
$\Delta^{13}C_a$				0.239	0.059	0.049	−0.029
$\delta^{18}O_a$					0.428***	0.186	0.192*
$\delta^{18}O_b$						0.030	−0.113
Quelccaya							0.387***

* Marginally significant relationship (p value < 0.1).
** Significant relationship (p value < 0.05).
*** Highly significant relationship (p value < 0.01).

($r = 0.381$, p value = 0.0002, DF = 121, and Table 2), indicating that a coherent $\delta^{18}O$ signal is incorporated throughout the annual growth rings in this tropical tree species as well (Figure 5). A marginally significant relationship was also observed between $\delta^{18}O_{cx}$ and annual ring width (Table 2). This observed negative relationship is consistent with theory, such that increased annual growth should be associated with depleted oxygen isotope values in wetter years. There were also marginally significant relationships between oxygen isotopes in the first radii ($\delta^{18}O_a$) and two nearby ice core records, as well as a marginally significant relationship between annual ring-width index and the Andean ice core index (Table 2).

In both tropical tree taxa sampled at our two study sites monthly precipitation values were positively correlated with annual ring width and negatively correlated with $\delta^{18}O_{cx}$. Both $\delta^{18}O_{cx}$ and annual ring width in *Cedrela odorata* showed a response to seasonal precipitation occurring from November to March of the current year (Figure 6a). Although strong correlations between precipitation and annual ring width are also apparent during June and August and significant correlations between precipitation and $\delta^{18}O_{cx}$ are evident in certain months from the previous year, there is a clear synchronous (and, in the case of $\delta^{18}O_{cx}$, highly significant) response in these proxies to monsoon precipitation of the current year. Similarly, in *Polylepis tarapacana* we see a synchronous response in correlations between $\delta^{18}O_{cx}$ and precipitation as well as annual ring width and precipitation (Figure 6b). The positive correlations between ring width and precipitation falling in December and January are suggestive of a positive growth response to monsoon precipitation. Furthermore, the negative correlation coefficients between $\delta^{18}O_{cx}$ and precipitation amount during rainy months are consistent with theory predicting more depleted oxygen isotopes with increased precipitation amount at these tropical sites.

To optimize models for predicting precipitation from our proxy measurements, we evaluated the relationship between individual proxies as well as combinations of proxies in capturing the variability of precipitation for various combinations of months. The optimal models selected for each tree species growing in each region are reported in Table 3. The optimal regression model for ring widths in *Cedrela*

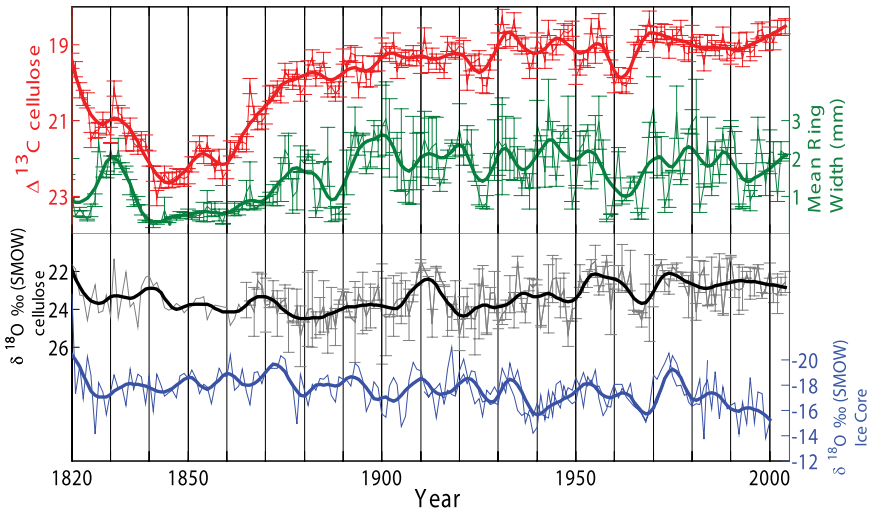

Figure 4. Carbon and oxygen isotopic values as well as mean annual ring width from *Cedrela odorata* compared with oxygen isotope values from a composite of Andean ice cores. Cellulose carbon isotope values (thin red) are plotted as the discrimination ($\Delta^{13}C$) against the $\delta^{13}C$ of atmospheric CO_2 (Francey et al. 1999) with error bars from instrumental precision and overlaid by a smooth spline function (thick red). Mean annual ring width is plotted for *Cedrela* (thin green) with error bars from the standard deviation between measurements and overlaid by a smooth spline function of the mean (thick green). Mean cellulose oxygen isotope values from two radial transects (thin gray) are plotted with error bars from the standard deviation between measurements and a smooth spline function (thick black). Plotted for comparison is a composite record of $\delta^{18}O$ ‰ AII (1910–2000; thin blue) from Hoffmann et al. (Hoffmann et al. 2003) and a portion of the Quelccaya ice core (1820–1984; thin blue) from Thompson et al. (Thompson et al. 1986) with a smooth spline function of the composite (thick blue). All oxygen isotope values are reported as $\delta^{18}O$ ‰ SMOW on inverted scales to reflect wetter conditions.

odorata was for precipitation in the months of December and January; however, this relationship was not significant (Table 3). The optimal model between $\delta^{18}O_{cx}$ in *Cedrela odorata* and precipitation was observed for the month of January, which was highly significant (p value = 0.000 59). The optimal multivariate model including ring width and $\delta^{18}O_{cx}$ in *Cedrela odorata* was for the months of December and January. Although this model shows a marginally significant relationship with precipitation, the relatively high value of AIC = 254.9 and the reduction in our cross-validation statistic ($X_{val} = 0.13$) suggest that combining $\delta^{18}O_{cx}$ and ring width in a single model does not increase our ability to predict precipitation at this site. In *Polylepis tarapacana*, annual ring width showed a significant positive relationship with December precipitation, whereas $\delta^{18}O_{cx}$ showed a significant negative relationship with March precipitation (Table 3). If we combine our proxies in a multivariate model, we are capable of predicting even more of the precipitation occurring in February and March (FM; $r = -0.44$, $p = 0.003$, DF = 53, and AIC = 233.15)

Table 2. Correlation matrix among proxies measured in two radii of *Polylepis tarapacana*, as well as previously published ice core $\delta^{18}O$ records. Pearson's correlation coefficients (*r*) between parameters are reported. Characteristics from *Polylepis* spp. (*N* = 122) are compared with $\delta^{18}O$ from the Quelccaya ice core (*N* = 106; Thompson et al. 1986) and the AII (*N* = 86; AII from Hoffmann et al. 2003). Oxygen isotope statistics are reported for two different radii from the same tree (subscripts a and b). Marginally significant and highly significant relationships are indicated.

	Ring-width index	$\delta^{18}O_a$	$\delta^{18}O_b$	Quelccaya	AII
Ring-width index		−0.206*	0.032	−0.043	−0.199*
$\delta^{18}O_a$			0.381**	0.228*	0.217*
$\delta^{18}O_b$				0.130	0.163
Quelccaya					0.387**

* Marginally significant relationship (p value < 0.1).
** Highly significant relationship (p value < 0.01).

and a cross-validation statistic ($X_{val} = 0.37$) that indicates very little loss in variance explained when random samples were removed from the regression model. Thus, this multivariate model incorporating $\delta^{18}O_{cx}$ and annual ring widths to predict February and March precipitation was selected as the optimal model.

We can then use these optimal models to reconstruct precipitation over these different tropical regions where precipitation data prior to 1950 are sparse or nonexistent. If we use $\delta^{18}O_{cx}$ in *Cedrela odorata* to predict January precipitation over the region near Puerto Maldonado, Peru, we see that the model is more accurate at predicting the central tendency of observed precipitation values than extreme values in precipitation and thus is not biased by anomalous precipitation values (Figure 7a). The model also predicts a slight decline in precipitation from 1820 to 1889 ($r = -0.66$, p value < 0.0001, and DF = 79) followed by a steady increase in precipitation from 1890 to 2004 ($r = 0.38$, p value < 0.0001, and DF = 104). Using chronologies of $\delta^{18}O_{cx}$ and annual ring width from *Polylepis tarapacana* to hindcast February and March precipitation over the Altiplano of Bolivia, we see a declining trend in precipitation since 1880 ($r = -0.43$, p value $<$ 0.0001, and DF = 118). There also appears to be coherent low-frequency climate variability evident in both precipitation records with apparent increases in monsoon precipitation around 1910 and 1930 (Figures 7a,b). However, more precipitation proxy chronologies are necessary to verify the regional extent of these apparent trends in tropical precipitation and their decadal variability in tropical precipitation.

Our reconstructions of monsoon precipitation share some temporal variability with Pacific sea surface temperature anomalies associated with ENSO (Figures 8a,c). These similarities are most evident when the time series are inspected in the frequency domain using the wavelet coherence transform. The high-frequency (low period) variability associated with ENSO is clearly evident in our reconstruction of January precipitation from the Peruvian Amazon. Especially strong coherence between ENSO and January precipitation was observed at periods <4 (frequencies greater 0.25 yr^{-1}), with significant coherence at these periods occurring in the 1870s, in the early 1900s, and from 1980 to 2000 (Figure 8b). Our reconstruction of precipitation for February and March in the Altiplano shows less of a correspondence with ENSO (Figure 8c); however, significant coherence

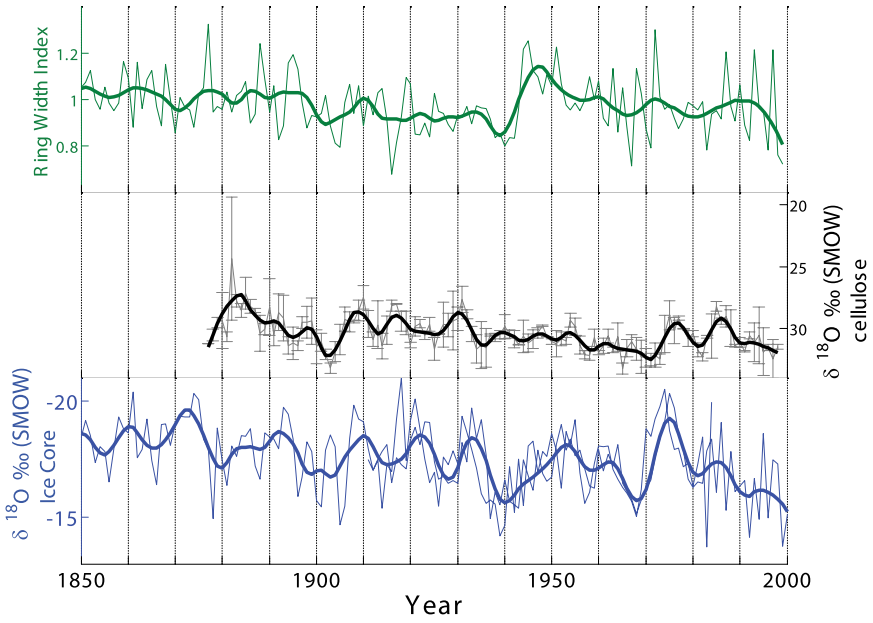

Figure 5. Oxygen isotope and ring-width time series from *Polylepis tarapacana* compared with oxygen isotope records from nearby Andean ice cores. Annual ring-width index (thin green) is plotted along with a smooth spline of the index (thick green). Mean cellulose $\delta^{18}O$ ‰ values from two radii (thin gray) are plotted with error bars representing the standard deviation and a smooth spline fit to their mean (thick black). Plotted for comparison is a composite of $\delta^{18}O$ ‰ records from Hoffmann et al.'s (Hoffmann et al. 2003) All (1910–2000; thin blue) and Thompson et al.'s (Thompson et al. 1986) Quelccaya ice core (1850–1984; thin blue). The ring-width index is the quotient of a spline function fit to the original data (Cook and Peters 1981). Note that all oxygen isotope data have been plotted as $\delta^{18}O$ ‰ SMOW and axes have been inverted such that negative values indicate wetter conditions.

between February and March precipitation in the Altiplano and the high-frequency variability associated with ENSO is apparent from 1950 to 1975 (Figure 8d). If we take the scores from the first principal component calculated from our proxy data (i.e., annual ring width and $\delta^{18}O_{cx}$) at both sites and compare it to ENSO variability, there are intervals of strong correspondence (Figure 9a). However, much of the coherence between these time series is at lower frequencies (high period) and only in the 1960s and 1980s does there appear to be significant coherence between ENSO and this more regionally integrated precipitation reconstruction (Figure 9b).

4.4. Spatial variability in precipitation inferred from tree-ring proxies

The regression models that we have optimized at each of our study sites can also be applied to infer regional patterns of precipitation variability. We can use our optimized model of $\delta^{18}O_{cx}$ in *Cedrela odorata* (Table 3) to infer spatial patterns of

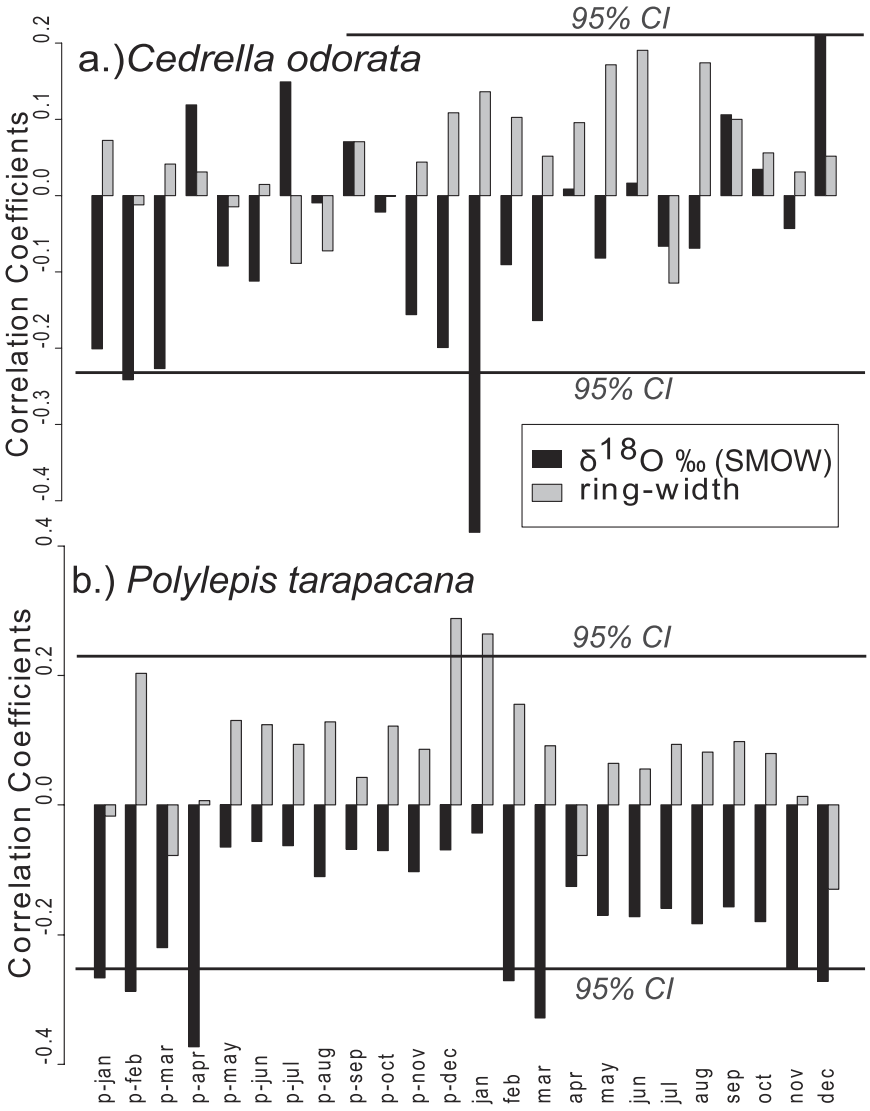

Figure 6. Correlation coefficients for linear regressions between tree-ring proxies and monthly precipitation for (a) *Cedrela odorata* and (b) *Polylepis tarapacana*. The mean of precipitation values was calculated from the four grid cells encompassing each study site from the updated global precipitation database (Dai et al. 1997). Precipitation data spanned 57 continuous years for *Cedrela* and 55 continuous years for *Polylepis*. Pearson correlation coefficients between monthly precipitation and mean annual observations of cellulose $\delta^{18}O$ (black) and ring width (gray) were calculated for the two taxa growing at the different study sites. Correlations between proxies and precipitation occurring in months of the preceding year are indicated by "p month." The 95% confidence intervals (CIs) are also plotted for *Cedrela* at $-0.22 < r < 0.22$ and for *Polylepis* at $-0.23 < r < 0.23$.

Table 3. Optimal regression models for statistical relationships between monthly precipitation and tree-ring proxy data. Optimal regression models were selected based on Pearson correlation coefficients (*r*), level of significance (*p* value), and the AIC. Cross-validation statistics (X_{val}) were also calculated as an independent measure for evaluating model predictions. The *y* intercepts (β_o), the slope parameters (β_1 and β_2), and SE± are also reported for each regression model, as well as the DF.

			Ring width		Cellulose $\delta^{18}O$			Model fit			
	β_o	SE±	β_1	SE±	β_2	SE±	r	p value	DF	AIC	X_{val}
Cedrela odorata											
January precipitation	18.03	3.62			−0.57*	0.16	−0.44	0.000 59	55	206.5	0.36
December–January precipitation	1.01	0.07	0.0002	0.0001			0.13	0.18	55	236.8	0.08
December–January precipitation	23.65	3.52	0.0001	0.0004	−0.56**	0.27	−0.29	0.09	54	254.9	0.13
Polylepis tarapacana											
March precipitation	30.71	9.99			−0.82*	0.32	−0.33	0.013	54	264.4	0.22
December precipitation	−0.66	2.75	6.30*	2.74			0.30	0.025	54	267.8	0.17
February–March precipitation	64.47	18.55	8.79*	4.69	−1.93*	0.59	−0.44	0.003	53	233.1	0.37

* Highly significant model parameter.
** Significant model parameter.

January precipitation in the Amazon lowlands. This analysis reveals strong correlations between $\delta^{18}O_{cx}$ and January precipitation along the eastern slope of the Andes, with the most significant correlations occurring in eastern Peru and Colombia (Figure 10a). This pattern is largely consistent with the degree of spatial autocorrelation occurring between local and regional precipitation at this site (Figure 10b). This spatial pattern suggests a coherent response in precipitation variability along the Andes that may reflect a common moisture source from the tropical Atlantic Ocean. In contrast, the optimized model for *Polylepis tarapacana* employing $\delta^{18}O_{cx}$ and annual ring width tends to capture precipitation occurring in the lowland Amazon basin during February and March, with the most significant correlation coefficients in lowland Bolivia and eastern Brazil (Figure 10c). Once again, this spatial pattern is fairly consistent with the spatial autocorrelation evident between local and regional precipitation (Figure 10d). These findings suggest a slightly different moisture source to the Altiplano, with some moisture coming from within the Amazon basin.

The scores extracted from the first principal component calculated from all of our proxy data from both sites was regressed over seasonal precipitation (JFM) falling over tropical South America (Figure 11). Patterns of spatial correlation evident between the first principal component and JFM precipitation bear a remarkable resemblance to patterns of precipitation variability associated with ENSO (Figure 1a), with regions of strong negative correlation evident in the northwestern portion of the Amazon basin and regions of strong positive correlation evident in the southeastern portion of the Amazon basin.

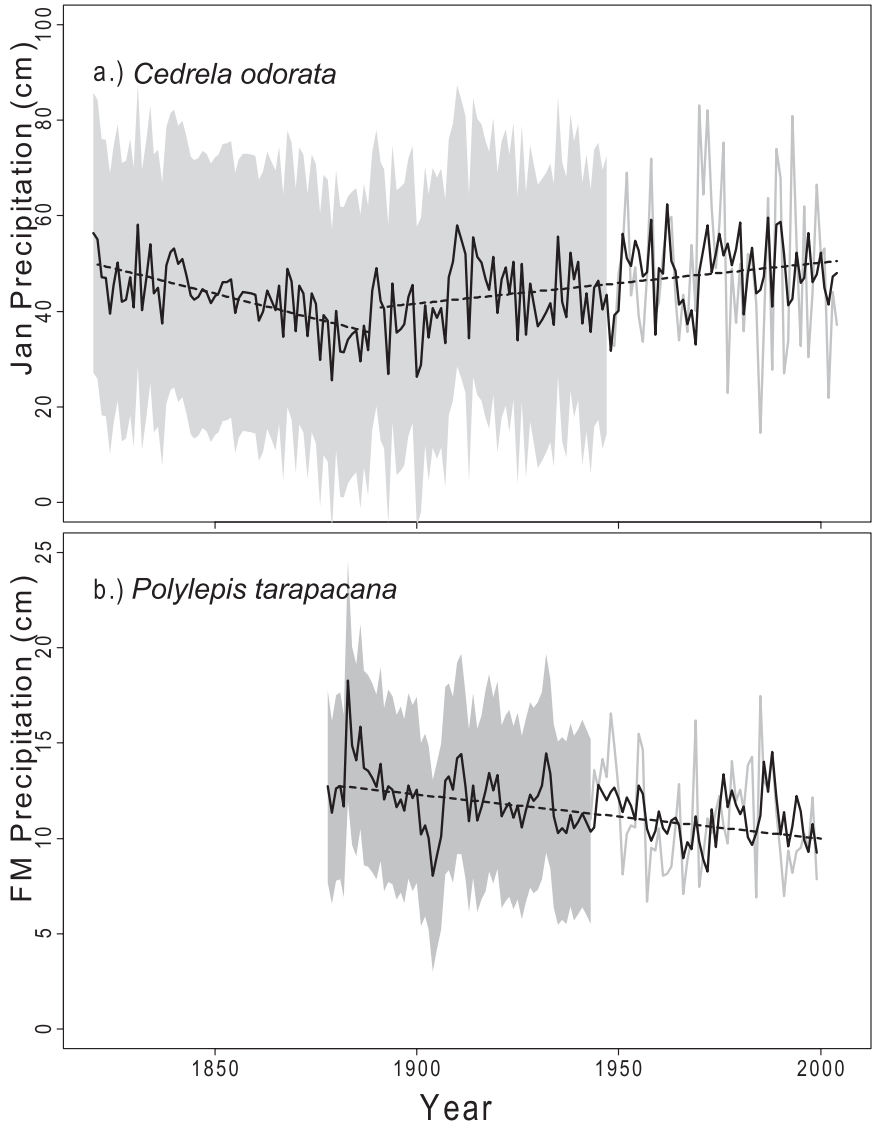

Figure 7. Reconstructing past precipitation based on optimal models for (a) *Cedrela odorata* and (b) *Polylepis tarapacana*. Models were optimized to hindcast observed instrumental precipitation (gray line) for (a) January in the Amazon and (b) FM in the Altiplano based on parameters reported in Table 2. These models were then used to reconstruct monthly precipitation over these tropical regions (black lines). The gray envelope represents the predicted CI for our precipitation reconstructions. Trend lines (broken black lines) have been added to the relationship between time and (a) January precipitation in *Cedrela* from 1820 to 1889 ($r = -0.66$; p value < 0.0001) and from 1890 to 2004 ($r = 0.38$; p value < 0.0001) and (b) FM precipitation for *Polylepis* ($r = -0.42$; p value < 0.0001).

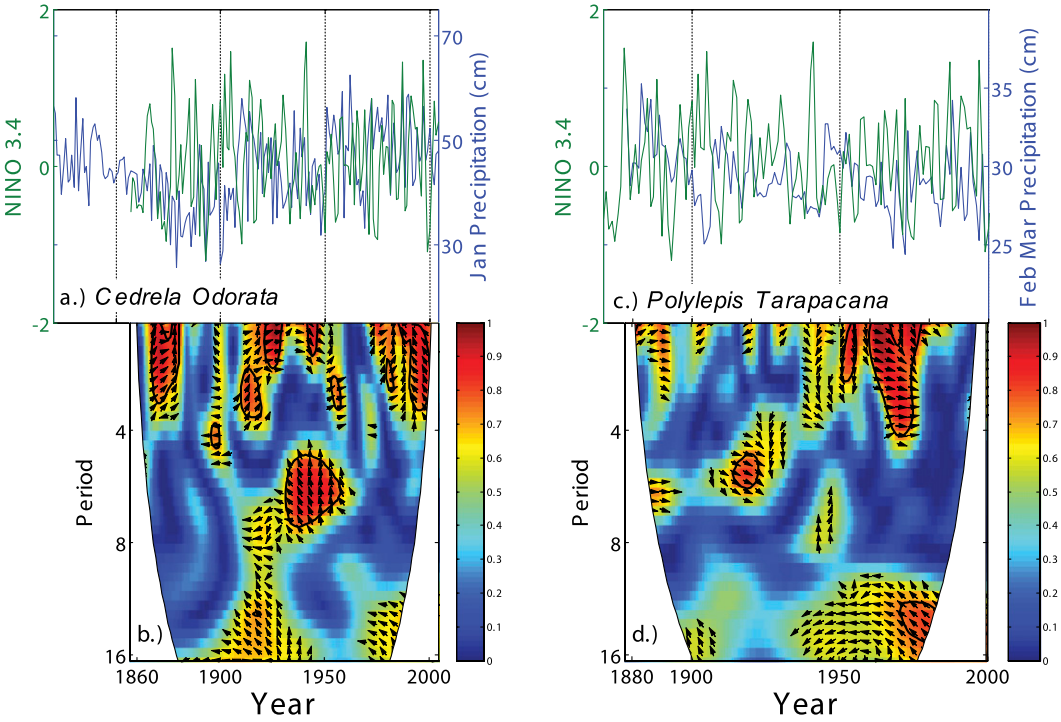

Figure 8. Wavelet coherence transform comparing shared frequency between reconstructed precipitation and El Niño SST anomalies: (a) January precipitation for Peruvian Amazon reconstructed from proxies in *Cedrela odorata* (blue) and (c) FM precipitation for the Atliplano reconstructed from proxies in *Polylepis tarapacana* (blue). Both reconstructions are plotted with the Niño-3.4 index averaged over JFM in green for comparison. (b),(d) The wavelet coherence illustrating temporal frequency coherence between the time series at given periods. Arrows indicate the phase relationship between series with in-phase pointing right and antiphase pointing left. The colors indicate the power of the spectrum at given periods. Intervals where time series share significant coherence in their power spectrum are delineated with a black line.

5. Discussion

5.1. Spatial patterns of ENSO, precipitation, and oxygen isotopes

A feature of the spatial correlation pattern relating Niño-3.4 and monsoon precipitation over tropical South America is the arc from the mouth of the Amazon River, westward across the Amazon basin, and southeastward toward Rio de Janeiro (Figure 1a). These negative correlation coefficients highlight the region of monsoon precipitation that is most sensitive to ENSO variability. This spatial pattern also follows the descending limb of the intertropical convergence zone (ITCZ) as it dips south during the South American monsoon (Münnich and Neelin 2005), indicating that ENSO may play an important role in regulating the advection of moisture into the Amazon. Our analysis focusing on the spatial relationship

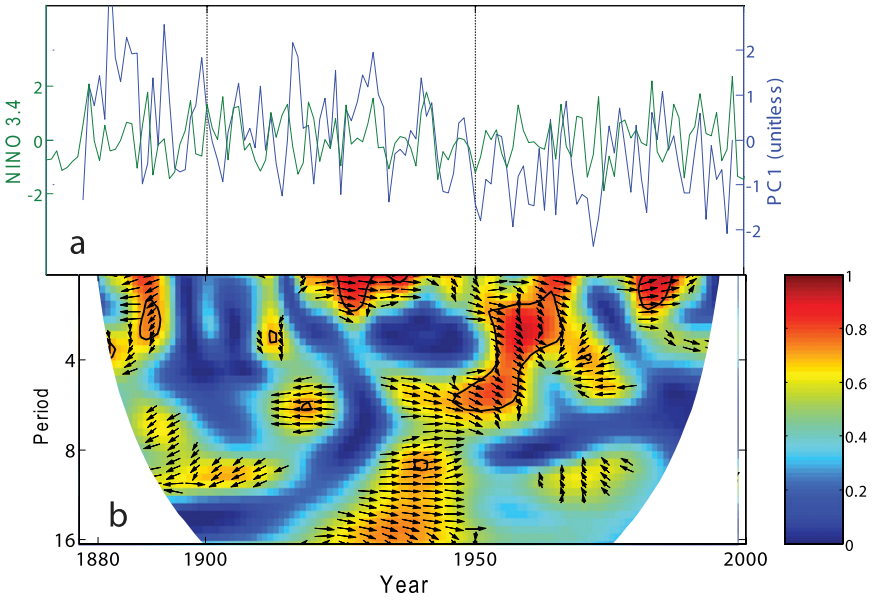

Figure 9. Wavelet coherence transform comparing shared frequency between the first principal component from our proxy data (blue) and average El Niño SST anomalies for JFM (Niño-3.4 in green). Proxy data included in our principal components analysis are the $\delta^{18}O_{cx}$ and ring-width data from *Polylepis* and $\delta^{18}O_{cx}$ data from *Cedrela* that are significantly correlated with seasonal precipitation (Table 3). (a) Raw data from both time series are plotted together for comparison and (b) the wavelet coherence transform. Arrows indicate the phase relationship between series with in-phase pointing right and antiphase pointing left. The colors indicate the power of shared coherence between frequencies in the two time series. Intervals where time series share significant coherence in their power spectrum are delineated with a black line.

between monsoon precipitation and ENSO has revealed patterns similar to previous analyses focusing on annual precipitation (Malhi and Wright 2004), with negative correlation coefficients in the northeastern and southeastern sectors of the Amazon and a lobe of positive correlation coefficients in the eastern sector of the basin centered over Bahia.

Monsoon precipitation is also well correlated with $\delta^{18}O_{sw}$ for several of the ENSO-sensitive regions of South America (Figure 1b). Our point-based correlation coefficients between $\delta^{18}O_{sw}$ and precipitation amount are largely consistent with spatial patterns based on a global analysis of $\delta^{18}O_{sw}$ presented by Bowen (Bowen 2008) and spatial patterns simulated using a general circulation model with isotopic tracers (Vuille et al. 2003). Of the 35 sampling sites included in our analysis, 5 sites experienced greater correlations when $\delta^{18}O_{sw}$ lagged precipitation by one to two months (see Table S1). This could be the result of hydrologic recycling within the Amazon as a result of transpiration, which would further deplete the $\delta^{18}O_{sw}$ of precipitation as it passes over the Amazon basin. In fact, it has been inferred from $\delta^{18}O$ measurements in precipitation that approximately 50% of the precipitation

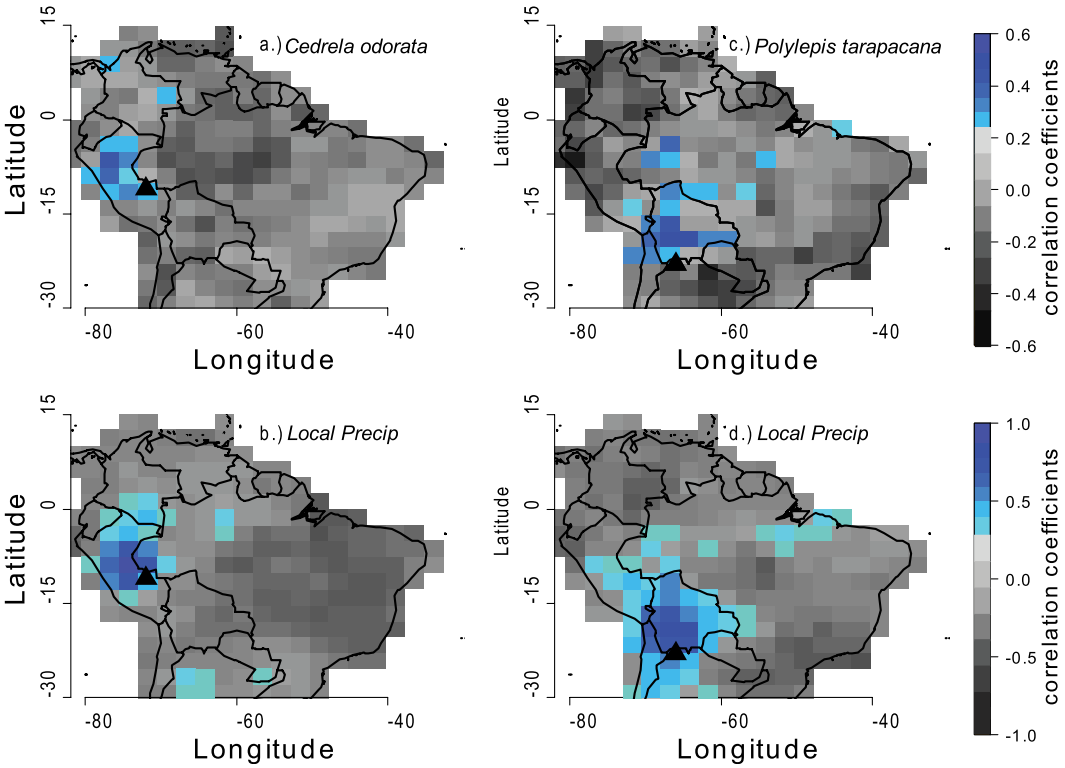

Figure 10. Spatial correlations between proxies and regional precipitation for tropical South America (Dai et al. 1997). Spatial correlation models are based on optimized regression models (Table 3). (a) Correlation coefficients plotted for *Cedrela odorata* are for $\delta^{18}O$ in cellulose and January precipitation. (b) These are compared to correlation coefficients of local and regional January precipitation for the Peruvian Amazon. (c) Correlation coefficients plotted for *Polylepis tarapacana* are for both $\delta^{18}O$ and ring-width chronologies and the sum of FM precipitation. (d) These are compared to correlation coefficients of local and regional precipitation falling in FM for the Altiplano. Grids plotted in color indicate significant correlations (p value < 0.05) for our *Cedrela* reconstruction $r > 0.22$ and for our *Polylepis* reconstruction $r > 0.23$. All correlation coefficients have been normalized such that positive values correspond with increased precipitation.

falling within the Amazon is recycled through evapotranspiration (Salati and Vose 1984). This may also explain the spatial covariance observed between our precipitation proxies in the Altiplano and more regional precipitation falling over the Amazon basin (Figure 10c). It has been shown that tap roots of some Amazon trees have access to deep groundwater (Nepstad et al. 1994) that may be out of equilibrium with the $\delta^{18}O$ of atmospheric water vapor. Thus, it is conceivable that water transpired by trees may be both out of phase and slightly isotopically enriched with respect to atmospheric water vapor.

Although there is an inverse correlation between $\delta^{18}O$ of precipitation and precipitation amount over most of the neotropics, correlation coefficients are fairly low,

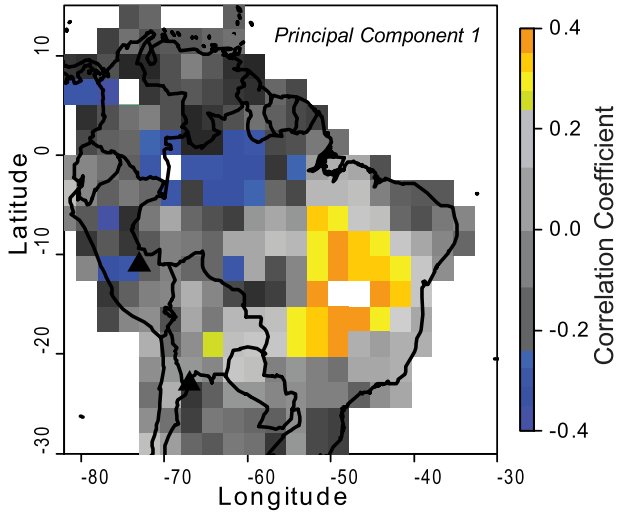

Figure 11. Spatial correlations between the first principal component of tree-ring proxies from both our sites and the sum of precipitation falling in JFM for tropical South America (Dai et al. 1997). Pearson correlation coefficients are plotted for each grid cell from 1880 to 2000. Colored grid cells indicate a significant relationship, and grayscale grid cells indicate no significant relationship. Precipitation values at each grid cell are correlated with the scores of the first principal component derived from annual measurements of ring width and oxygen isotopes measured at both study sites.

even at optimal sites ($-0.8 < r < -0.6$). Thus, even if trees growing at these optimal sites were perfect recorders of isotopes in precipitation, only about 40%–60% of the precipitation variability could be explained by $^{18}O_{cx}$ alone. Although this statistical relationship rivals that of proxies used to reconstruct temperature at high latitudes (Jones and Mann 2004), it is slightly less than ring-width chronologies used to reconstruct drought at high latitudes (Cook et al. 2004). Therefore, oxygen isotopes in tropical trees may be useful for reconstructing precipitation in other parts of the Amazon basin where precipitation data are sparse or nonexistent. Finally, $\delta^{18}O_{cx}$ measurements in tropical trees can be combined with ring-width measurements in precipitation-sensitive taxa as demonstrated in this study to explain more variability in modern precipitation and gain greater confidence in reconstructing past precipitation variability. A similar approach has been taken for investigating changes in precipitation in Pakistan, where both annual ring width and $\delta^{18}O_{cx}$ of juniper trees were found to be significantly correlated with seasonal precipitation (Treydte et al. 2006), despite this subtropical location where there is not a particularly strong correlation between $\delta^{18}O_{sw}$ and precipitation (Bowen 2008).

5.2. Chronology and seasonal isotopic variability

Although it is true that there is little seasonal fluctuation in tropical temperatures, this is not true for precipitation and, as we have demonstrated, the growth of some tropical tree species may be sensitive to seasonal fluctuations in precipitation.

In fact, during an experimental drought in the central Amazon, net primary productivity was reduced by 25% (Nepstad et al. 2002). The annual ring widths in both *Polylepis* spp. (Morales et al. 2004) and *Cedrela* spp. (Dunisch et al. 2003) have been previously correlated with precipitation variability. Even though net ecosystem carbon uptake (Saleska et al. 2003) and remotely sensed metrics of primary productivity (Huete et al. 2006) indicate an increase in net ecosystem productivity during the dry season, possibly due to enhanced light availability (Graham et al. 2003), the accrual of woody biomass appears to occur primarily during the rainy season (Saleska et al. 2003). It is possible that changes in the growth rate of tropical trees measured by dendrometer bands are due to the swelling and contraction of xylem in response to transpiration. Although this has been observed on diurnal time scales, it is unlikely to account for the factor of 5 increase in seasonal growth rates of *Tachigali* spp. observed in this study (see Figure 3) and the differential seasonal growth observed in an extensive study of tree growth in the central Amazon (da Silva et al. 2002).

Extensive research has been done on *Polylepis*, growing in the central Andes, suggesting that growth rings are annual and are sensitive to the amount of seasonal precipitation (Christie et al. 2009; Morales et al. 2004; Solíz et al. 2009). The annual chronology of *Polylepis* has been verified by our independent measurements of $\Delta^{14}C$, and thus the annual ring widths and isotopic composition of *Polylepis* may provide independent proxies of interannual climate variability. On the other hand, our $\Delta^{14}C$ measurements of *Cedrela* suggest that the growth rings in *Cedrela* may in fact be annual, but further research should be conducted to cross-date individuals and generate regional climate reconstructions of the Peruvian Amazon, similar to studies using *Cedrela* to reconstruct climate in northern Argentina (Villalba et al. 1992). The revised extraction technique (Brendel et al. 2000) employed in our study apparently introduced modern carbon to the samples that was not removed during the additional rinse step. Previous studies employing the Brendel extraction method also encountered some difficulty when trying to date samples using ^{14}C (Evans and Schrag 2004; Poussart et al. 2004). All of the samples that we extracted and analyzed for $\delta^{13}C_{cx}$ consistently yielded the 40%–45% carbon per total mass of sample that is expected for cellulose, suggesting that the Brendel method may be reliable for stable isotopic studies. Our experience is consistent with the conclusion of a recent comparison of several cellulose-extraction methods suggesting that the Brendel method is suitable for stable isotopic analysis but may lead to erroneous ^{14}C dates because of contamination (Gaudinski et al. 2005). Both Gaudinski et al. (Gaudinski et al. 2005) and Anchukaitis et al. (Anchukaitis et al. 2008a) concluded that contamination in the Brendel method is due to a ^{14}C-depleted source; however, our results suggest that the modified Brendel technique employed here resulted in the addition of modern carbon as evidenced by the detection of ^{14}C in our ^{14}C dead internal standard. Unfortunately, neither Gaudinski et al. (Gaudinski et al. 2005) nor Anchukaitis et al. (Anchukaitis et al. 2008a) included a ^{14}C dead standard in their comparison of methods, so it is impossible to determine the exact source of carbon contamination in our samples. The most likely explanation is the cross-contamination among our samples, whereby modern ^{14}C was introduced from our samples to our standard and ^{14}C dead carbon was introduced from our standard to our samples, which would explain the presence of modern ^{14}C in our ^{14}C dead standard and the slightly biased depleted $\Delta^{14}C$ values observed in our samples (Figure 2). Nevertheless, the cross-dated ring-width

chronologies and ^{14}C dates (RMSE = ±2.0) indicate that the growth rings in *Polylepis tarapacana* are annual. Although clear growth rings are evident in *Cedrela odorata*, further research is required to develop annually resolved chronologies from this taxa growing in the Amazon.

By taking advantage of a long-term growth study of Amazon trees, we were able to validate the intra-annual cycle of $\delta^{18}O_{cx}$ and its correspondence with growth and precipitation. The time series of $\delta^{18}O_{cx}$ captures three growth seasons, in which there is a significant relationship between minima in $\delta^{18}O$ and maxima in precipitation. It has been hypothesized that the seasonal cycle of $\delta^{18}O_{cx}$ may be used to infer an annual growth chronology in tropical trees lacking annual rings. Our direct measurements of monthly growth rate and high-resolution $\delta^{18}O_{cx}$ provide direct empirical evidence that this approach is valid, at least for *Tachigali* spp. growing in Manaus. However, additional paired measurements of $\delta^{18}O_{cx}$ and in situ growth rate are necessary to substantiate this relationship in more tropical taxa over broader regions and during known drought events.

The annual distribution of historical observations of $\delta^{18}O_{sw}$ in precipitation from Manaus (IAEA; 1956–92) reveals greater seasonal amplitude (range ≈ 10‰) than our values of $\delta^{18}O_{cx}$ measured in *Tachigali* spp. (range ≈ 5‰). One possible explanation for this attenuated seasonal cycle in $\delta^{18}O_{cx}$ is that this particular tree is growing at a faster rate during the summer months between December and March (Figure 3) and thus is biased in its sampling of precipitation during these wetter months, which actually have a slightly reduced range in $\delta^{18}O$ values (DJFM range ≈ 7‰). It is also possible that increased evaporative enrichment may be occurring during the dry season when $\delta^{18}O_{sw}$ is relatively depleted, thereby causing the seasonal cycle to become attenuated (Roden et al. 2000). An alternative explanation is that this individual may be integrating water that is not exclusively falling during months of the growth season by relying on deeper water with a slightly different isotopic signature. It has been shown that certain Amazonian trees have very deep taproots that are capable of accessing water from a soil depth of 8 m (Nepstad et al. 1994) and redistributing this water to meet photosynthetic demands during the dry season (Oliveira et al. 2005). This utilization of deep groundwater is also suggested by the high correlation between monthly growth rates and long-term climatological monthly means of precipitation (da Silva et al. 2002). Thus, seasonal changes in growth rate and access to deep groundwater during periods of drought stress may alter fluctuations in $\delta^{18}O_{sw}$ that are due to precipitation amount. Finally, the apparent trend of more depleted $\delta^{18}O_{cx}$ values in *Tachigali* growing in Manaus could be indicative of an increase in total precipitation at the site. Although long-term records of precipitation at Manaus show a significant increase in precipitation over the last 40 years (Haylock et al. 2006), it is not possible to discern this trend over the limited duration of our isotopic record and longer records of isotopes in trees growing at Manaus would be necessary to reconstruct changes in precipitation prior to the instrumental record.

5.3. Temporal variability in tree-ring proxies and precipitation

Having established that these taxa have annual growth rings and that intra-annual growth and isotopic variability are sensitive to precipitation amount, it is

important to verify that the temporal variability of $\delta^{18}O_{cx}$ recorded in different radii of the same tree are coherent. The $\delta^{18}O_{cx}$ series measured in two separate radii from the *Polylepis* sample were significantly correlated, as were the time series of $\delta^{18}O_{cx}$ measured in *Cedrela* (Tables 1 and 2). A similar study investigating the isotopic variability in *Podocarpus neriifolius*, a tropical taxa growing in Thailand (Poussart et al. 2004), found a more coherent $\delta^{18}O_{cx}$ signal between radii ($0.5 < r < 0.7$). However, *Podocarpus neriifolius* does not have annual growth rings, and therefore correspondence between the two $\delta^{18}O_{cx}$ time series was optimized to yield a maximum correlation. Nevertheless, these independent studies conducted on different tropical tree taxa in separate regions suggest that a coherent $\delta^{18}O_{cx}$ signal can be extracted from the cellulose of tropical trees. However, these results should be corroborated by more replication of time series from other trees from the same region to determine if the isotopic signal recorded in tropical trees is coherent between trees and over broader scales.

Our time series of isotopic and ring-width variability generated from *Cedrela odorata* in the Amazon also revealed significant correlations with regional monsoon precipitation but with some subtle differences. In *Cedrela odorata*, the relationship between $\delta^{18}O_{cx}$ and monsoon precipitation was much stronger (Figure 6a), with maximum correlations occurring with January precipitation. Only a weak relationship was observed between annual ring width and monsoon precipitation. However, this was not surprising, given the fact that only one individual of *Cedrela odorata* was analyzed in this study. Previous studies have demonstrated a strong relationship between annual ring width in *Cedrela odorata* and seasonal precipitation in northern Argentina (Villalba et al. 1992). To our knowledge, this is the first ring-width series generated from *Cedrela odorata* in the Amazon of Peru. By combining our ring-width series with other ring-width series into a regional ring-width chronology, changes in precipitation could be inferred for this very important climatological region with sparse instrumental data. If we use the significant relationship between $\delta^{18}O_{cx}$ in *Cedrela* and January precipitation to hindcast regional precipitation, we see a declining trend in January precipitation until about 1890 followed by an apparent increasing trend in January precipitation over the twentieth century. This is consistent with observations that show an increase in global precipitation due to human influence, especially for tropical latitudes between 0° and 30°S (Zhang et al. 2007). However, these results initially appear to be at odds with the regional analysis of Haylock et al. (Haylock et al. 2006) that shows a significant decline in precipitation for the lowland regions of Peru. However, the analysis of Haylock et al. (Haylock et al. 2006) was based on the analysis of data spanning the years 1960–2000, which is a period of very little appreciable change in our precipitation reconstruction and an apparent decline in precipitation from the instrumental record (Figure 7a). This clearly illustrates the lack of climate data as well as the need for more climate reconstructions from this very important region.

The most significant and unexpected relationship to emerge among parameters measured in *Cedrela odorata* was the inverse correlation between $\Delta^{13}C$ and mean ring width. This relationship is most evident during the suppressed growth from 1830 to 1870, when discrimination values peaked. Because mean ring width and $\Delta^{13}C$ are temporally covariant, we might conclude that both have responded to a common climatic stimulus. However, the lack of a similar response in $\delta^{18}O_{cx}$ suggests that there may have been no major changes in precipitation amount during

this period. Instead, a more likely explanation for this covariance is that there was either a change in the source of CO_2, reflected in the value of $\delta^{13}C_{atm}$, or else that factors affecting growth also affected physiology through c_i/c_a. In fact, it is known that there is a large vertical gradient in $\delta^{13}C_{atm}$ within the canopy of tropical rain forests as a result of soil respiration (Buchmann et al. 1997a). Observed values of $\delta^{13}C_{atm}$ at the forest floor of 4‰ less than values at the top of the canopy are large enough to explain the apparent 3‰ deviation observed in our record of $\delta^{13}C_{cx}$. These results suggest that a certain fraction of respired CO_2 may be recycled within the canopy of tropical forests. Although people have speculated about this so-called cyclic enrichment $^{12}CO_2$ (Keeling 1961), there is little empirical evidence for its occurrence. Moreover, the slightly diminished cellulose $\Delta^{14}C$ values that appear to lag the peak in atmospheric $\Delta^{14}C$ by several years also indicate that older respired CO_2 may be refixed by the canopy in this forest. However, it has been demonstrated in a temperate forest that only 20% of the vertical isotopic gradient in vegetation can be explained by changes in the isotopic source of CO_2, whereas as much as 80% can be explained by a decreasing c_i/c_a with canopy height due to changes in photosynthetic rates (Buchmann et al. 1997b). A similar increase in isotopic discrimination has been identified under reduced-light conditions in Scandinavian pine trees (Gagen et al. 2007). Although our observations of $\Delta^{13}C$ from *Cedrela odorata* are from a completely different ecosystem, it is possible that decreased light availability due to canopy shading may have limited photosynthesis leading to suppressed growth. This decrease in photosynthesis would have caused internal CO_2 concentrations to increase (i.e., increased c_i/c_a) resulting in an increase in isotopic discrimination, which is what we observe in our record of $\Delta^{13}C$ from *Cedrela odorata*. Alternatively, it has been suggested that earlywood is slightly enriched in $\delta^{13}C_{cx}$ relative to latewood and that, during periods of reduced growth, earlywood is diminished, leading to a more depleted value of $\delta^{13}C_{cx}$ (Li et al. 2005). Such an effect would lead to greater apparent isotopic discrimination (i.e., increased $\Delta^{13}C$) during periods of reduced growth, which is also consistent with our observations. Unfortunately, there was no apparent difference in color or density between early and latewood in *Cedrela odorata*, so we did not make intra-annual measurements of $\delta^{13}C_{cx}$, but the intra-annual variability of $\delta^{13}C_{cx}$ and its relevance to seasonal physiological response should be further explored. Based on these observations, records of $\Delta^{13}C$ probably reflect local processes affecting the source of atmospheric CO_2, light availability, and the physiology of cellulose synthesis more than they reflect regional climatic processes.

The range of $\delta^{18}O_{cx}$ values (~2‰) in *Polylepis* appears to be attenuated compared with the range of $\delta^{18}O_{cx}$ values (~5‰) observed in ice cores from the central Andes. In fact, many of the minima in $\delta^{18}O$ apparent in the ice core record (e.g., 1870, 1910, 1955, and 1975) are also evident in our record of $\delta^{18}O_{cx}$ (Figure 4), which is evidenced by a weak correlation between oxygen isotope records in these alpine tree species and nearby ice cores. If the trees investigated in this study are recording similar values of $\delta^{18}O_{sw}$ as those recorded by ice core records, then this indicates that considerable evaporative enrichment has probably occurred in our tree-ring records of $\delta^{18}O_{cx}$. There also appears to be a weak correlation between the regional ring-width index and an index of $\delta^{18}O$ in ice cores. These preliminary results suggest that more extensive sampling of *Polylepis* and their oxygen isotopic composition may result in a tighter link between tree-ring proxies of precipitation

and ice cores, thereby improving our understanding of spatial and temporal variability in tropical precipitation.

The regional ring-width index generated for *Polylepis* was highly correlated with monsoon precipitation, especially for the month of December. This relationship between annual growth in *Polylepis* spp. and monsoon precipitation has been previously reported (Morales et al. 2004). Oxygen isotopes in *Polylepis* also showed a strong relationship with monsoon precipitation, with significant correlations occurring slightly later in February and March. This apparent lag between optimal correlations in our proxies could be due to lags in seasonal snowmelt coming from upslope that is utilized by *Polylepis* during photosynthesis. This reliance on snowmelt is also suggested by previous studies of *Polylepis* showing a significant relationship between growth and precipitation falling in the previous year (Morales et al. 2004). Nevertheless, if we combine these proxies into a single model, we are able to capture even more of the variability in monsoon precipitation occurring in February and March (Figure 7b). Our reconstruction of monsoon precipitation at this site reveals a declining trend in precipitation from around 1880 until the present. These results show the opposite trend from the increase in monsoon precipitation inferred from the proxies at our Amazon site (Figure 7a). These contradictory empirical results may provide support for the enhanced Hadley cell circulation commonly observed in model simulations in response to anthropogenic warming (Allen and Ingram 2002). Model simulations often indicate an increase in tropical precipitation, with more vigorous convection associated with the ascending limb of Hadley cells, but a decrease in subtropical precipitation, with the subsidence of drier air associated with the descending limb of the Hadley cell. Similar reconstructions of long-term precipitation variability may be helpful for testing model simulations and their ability to capture the response of tropical precipitation to anthropogenic warming (Zhang et al. 2007).

The cross-wavelet transform analysis indicated that January precipitation variability inferred from $\delta^{18}O_{cx}$ in *Cedrela odorata* was highly sensitive to ENSO variability during most of the twentieth century (Figure 8b). However, this coherence is much more significant and tends to be more in phase from 1860 to 1950. Since 1975, there is significant coherence between precipitation and ENSO variability, but these records appear to be 90° out of phase with ENSO variability leading precipitation variability. This coincides with the well-documented shift in ENSO to a more low-frequency regime after 1975 (An and Wang 2000). An and Wang (An and Wang 2000) suggested that this shift in ENSO structure coincided with an eastward shift of the westerly anomalies and a slackening of the easterlies. Although this shift in ENSO structure may have affected regional precipitation patterns, it does not necessarily explain the variability in phase at decadal time scales observed in our proxy record, and further research is required to identify the physical mechanisms controlling the transient ENSO signal evident in our proxy record. The teleconnection between ENSO variability and the position of the ITCZ over the tropical Atlantic is well established (Münnich and Neelin 2005). It has also been documented that the ITCZ has been gradually advancing northward for the past 400 years, possibly in response to anthropogenic warming (Sachs et al. 2009). Therefore, the position of the ITCZ may vary interannually in response to ENSO and may vary on longer time scales because of perturbations in Earth's radiative budget. Because the ITCZ is the primary mechanism for advecting moisture to the

Amazon and transmitting the ENSO signal to our site, slight changes in the position of the ITCZ over longer time scales could explain why ENSO variability is not consistently recorded by our proxies and interannual changes in the ITCZ may explain the emergent phase shifts between our precipitation reconstruction and ENSO variability.

The declining trend in monsoon precipitation in conjunction with the increased sensitivity to ENSO variability inferred from our proxies in the Altiplano suggest that this high-elevation site located on the southern margin of the tropics may be especially sensitive to perturbations to the tropical hydrologic cycle. Although there is significant coherence shared between January precipitation and ENSO, much of this coherence is at a higher frequency than the dominant frequency associated with ENSO observed over the last century (~4-yr period). This indicates that our multiproxy reconstruction may be more sensitive to the high-frequency interannual variability in precipitation associated with the shift between El Niño and La Niña events rather than the lower-frequency variability typically associated with ENSO.

Neither one of our proxy sites showed a significant and consistent correspondence with ENSO variability, but rather both sites demonstrated intervals over which ENSO events were faithfully recorded. We suspect that this may be symptomatic of many paleoclimatic studies that attempt to capture nonstationary atmospheric processes, such as ENSO, using stationary proxy data, such as tree rings or corals. In fact, when we extract the first principal component from our two climate reconstructions, there appears to be stronger and more consistent temporal correspondence with ENSO variability (Figure 9). Thus, our results indicate that a network of multiproxy tree reconstructions would be most effective at reconstructing ENSO variability as transmitted through tropical precipitation variability.

5.4. Spatial patterns in precipitation inferred from tree-ring proxies

Our spatial analysis revealed different sources and trajectories for seasonal precipitation at our two study sites. The $\delta^{18}O_{cx}$ of *Cedrela odorata* growing in the Peruvian lowlands was highly correlated with January precipitation occurring along the eastern slope of the Andes (Figure 10a). Both $\delta^{18}O_{cx}$ and annual ring widths in *Polylepis tarapacana* were correlated with February and March precipitation in the lowlands of Bolivia in Brazil, suggesting that a fraction of the precipitation falling on the Altiplano may actually be recycled water due to precipitation and subsequent evapotranspiration in the Amazon basin. This analysis suggests that the recycling of water within the Amazon (Salati and Vose 1984) may actually affect the amount of seasonal precipitation occurring in the adjacent Andes, which is corroborated by the lags observed between $\delta^{18}O$ minima and precipitation maxima for some IAEA stations on the eastern edge of the Amazon basin (Table S1). Finally, spatial correlations between the first principal component of our proxy data combined from both sites and regional precipitation showed a highly polar pattern (Figure 11) that bears a remarkable resemblance to the relationship between El Niño anomalies and monsoon precipitation falling over tropical South America (Figure 1a). The coherence between these spatial patterns suggests that a network of tropical trees could be used to reconstruct spatial

patterns of precipitation across the Amazon and how they respond to changes in El Niño intensity.

6. Conclusions

In summary, our results provide evidence that the growth and oxygen isotopic content of cellulose in certain tropical tree taxa is responsive to the amount of precipitation and that the sensitivity of these two proxies can be used to reconstruct precipitation. By investigating monthly growth rates and the intra-annual variability of $\delta^{18}O_{cx}$ in *Tachigali myrmecophila* growing in Manaus, Brazil, we verified that $\delta^{18}O_{cx}$ values do in fact vary on seasonal time scales. This seasonal variability in $\delta^{18}O_{cx}$ also corresponds with seasonal patterns of precipitation amount. Thus, the number of $\delta^{18}O_{cx}$ seasonal cycles can be used to infer chronology and the amplitude of $\delta^{18}O_{cx}$ seasonal cycles can be used to infer precipitation amount in certain tropical tree taxa without annual growth rings growing in certain environments.

We found that *Cedrela odorata* growing in the Peruvian Amazon clearly exhibit ring widths that are correlated with seasonal precipitation; however, further research must be done to corroborate that the ring widths evident in *Cedrela odorata* are in fact annual and that annual growth is responsive to seasonal precipitation on a more regional scale. We also found that oxygen isotopes within the cellulose of *Cedrela odorata* ring widths were negatively correlated with seasonal precipitation, which is consistent with isotopic theory. These results, combined with previous observations of annual ring widths in *Cedrela odorata*, indicate that it may be possible to extend limited instrumental records of precipitation for the Amazon by investigating multiple proxies in this ubiquitous and long-lived neotropical tree species. Our results from *Polylepis tarapacana* were the most promising and indicated that ring widths could be used in conjunction with $\delta^{18}O_{cx}$ to reconstruct regional precipitation. Our results also suggest that *Polylepis tarapacana* growing in the Altiplano may also be sensitive to changes in precipitation patterns modulated by ENSO variability; however, similar records of oxygen isotopes and ring widths must be derived from other *Polylepis tarapacana* growing in this region to identify the impacts of ENSO variability on the spatial heterogeneity of precipitation. The carbon isotopic variability in the cellulose of some tropical trees may reflect changes in source CO_2 or changes in physiology due to local processes rather than regional climatic processes. Thus, $\Delta^{13}C$ records derived from tropical trees should be interpreted with caution and should only be compared with climate records when the life history and site dynamics are well understood.

This study emphasizes the importance of multiple proxies in quantifying past climatic variability. Some proxies may be more responsive than other proxies at certain sites, and increased predictive power can be gained by including several proxies of the same climatological phenomenon in a multivariate statistical framework. Furthermore, multiproxy climate records derived from tropical trees may prove critical in extending the spatial and temporal extent of instrumental data in the tropics. Finally, a more extensive network of tree-ring isotope studies in the tropics could improve our understanding of the regional responses of the tropical hydrological cycle to important modes of climate variability, such as ENSO (Lyon 2004) and anthropogenic warming (Zhang et al. 2007).

Acknowledgments. We thank Niro Higuchi from the Instituto Nacional de Pesquisas da Amazônia for the frequent measurements of trees growing at Manaus and Jaime Semizo of the World Wildlife Fund for assistance in Puerto Maldonado, Peru. Assistance with the enumeration of ring widths and extraction of cellulose was provided by Michael Evans and Steve Leavitt from the Laboratory of Tree Ring Research, University of Arizona. All stable isotopic analyses were performed by Jonathan Karr at the Duke Environmental Isotope Laboratory. Finally, we thank Tom Guilderson of the Lawrence Livermore Center for Accelerator Mass Spectrometry for generously offering to analyze ^{14}C samples for us. Previous versions of this manuscript were greatly improved by comments from Nigel Pitman, Miles Silman, and two anonymous reviewers. All raw proxy data reported herein have been uploaded to NOAA's National Climate Data Center Web site (available online at http://www.ncdc.noaa.gov/oa/ncdc.html).

References

Allen, M. R., and W. J. Ingram, 2002: Constraints on future changes in climate and the hydrologic cycle. *Nature,* **419,** 224–232.

An, S. I., and B. Wang, 2000: Interdecadal change of the structure of the ENSO mode and its impact on the ENSO frequency. *J. Climate,* **13,** 2044–2055.

Anchukaitis, K. J., M. N. Evans, T. Lange, D. R. Smith, S. W. Leavitt, and D. P. Schrag, 2008a: Consequences of a rapid cellulose extraction technique for oxygen isotope and radiocarbon analyses. *Anal. Chem.,* **80,** 2035–2041.

——, ——, N. T. Wheelwright, and D. P. Schrag, 2008b: Stable isotope chronology and climate signal calibration in neotropical montane cloud forest trees. *J. Geophys. Res.,* **113,** G03030, doi:10.1029/2007JG000613.

Borella, S., M. Leuenberger, and M. Saurer, 1999: Analysis of $\delta^{18}O$ in tree rings: Wood-cellulose comparison and method dependent sensitivity. *J. Geophys. Res.,* **104,** 19 267–19 273.

Bowen, G. J., 2008: Spatial analysis of the intra-annual variation of precipitation isotope ratios and its climatological corollaries. *J. Geophys. Res.,* **113,** D05113, doi:10.1029/2007JD009295.

Brendel, O., P. P. M. Iannetta, and D. Stewart, 2000: A rapid and simple method to isolate pure α-cellulose. *Phytochem. Anal.,* **11,** 7–10.

Buchmann, N., J.-M. Guehl, T. S. Barigah, and J. R. Ehleringer, 1997a: Interseasonal comparison of CO_2 concentrations, isotopic composition, and carbon dynamics in an Amazonian rainforest (French Guiana). *Oecologia,* **110,** 120–131.

——, W.-Y. Kao, and J. Ehleringer, 1997b: Influence of stand structure on carbon-13 of vegetation, soils, and canopy air within deciduous and evergreen forests in Utah, United States. *Oecologia,* **110,** 109–119.

Buckley, B., K. Palakit, K. Duangsathaporn, P. Sanguantham, and P. Prasomsin, 2007: Decadal scale droughts over northwestern Thailand over the past 448 years: Links to the tropical Pacific and Indian Ocean sectors. *Climate Dyn.,* **29,** 63–71.

Christie, D. A., A. Lara, J. Barichivich, R. Villalba, M. S. Morales, and E. Cuq, 2009: El Niño-Southern Oscillation signal in the world's highest-elevation tree-ring chronologies from the Altiplano, Central Andes. *Palaeogeogr. Palaeoclimatol. Palaeoecol.,* **281,** 309–319.

Cook, E. R., and K. Peters, 1981: The smoothing spline: A new approach to standardizing forest interior tree-ring width series for dendroclimatic studies. *Tree-Ring Bull.,* No. 41, 45–53.

——, and R. L. Holmes, 1984: Program ARSTAN user manual. University of Arizona Laboratory of Tree Ring Research, 9 pp.

——, C. A. Woodhouse, C. M. Eakin, D. M. Meko, and D. W. Stahle, 2004: Long-term aridity changes in the western United States. *Science,* **306,** 1015–1018.

Dai, A., I. Y. Fung, and A. D. Del Genio, 1997: Surface observed global land precipitation variations during 1900–88. *J. Climate,* **10,** 2943–2962.

Dansgaard, W., 1964: Stable isotopes in precipitation. *Tellus,* **16,** 436–468.

da Silva, R. P., J. dos Santos, E. S. Tribuzy, J. Q. Chambers, S. Nakamura, and N. Higuchi, 2002: Diameter increment and growth patterns for individual tree growing in central Amazon, Brazil. *For. Ecol. Manage.,* **166,** 295–301.

D'Arrigo, R., and Coauthors, 2006: Monsoon drought over Java, Indonesia, during the past two centuries. *Geophys. Res. Lett.,* **33,** L04709, doi:10.1029/2005GL025465.

Dunisch, O., V. Ribeiro Montóia, and J. Bauch, 2003: Dendroecological investigations on *Swietenia macrophylla* King and *Cedrela odorata* L. (Meliaciae) in the central Amazon. *Trees,* **17,** 244–250.

Enquist, B. J., and A. J. Leffler, 2001: Long-term tree ring chronologies from sympatric tropical dry-forest trees: Individualistic responses to climatic variation. *J. Trop. Ecol.,* **17,** 41–60.

Evans, M. N., and D. P. Schrag, 2004: A stable isotope-based approach to tropical dendroclimatology. *Geochim. Cosmochim. Acta,* **68,** 3295–3305.

Farquhar, G. D., J. R. Ehleringer, and K. T. Hubick, 1989: Carbon isotope discrimination and photosynthesis. *Annu. Rev. Plant Physiol. Plant Mol. Biol.,* **40,** 503–537.

Fonseca, C. R., and W. W. Benson, 2003: Ontogenetic succession in Amazonian ant trees. *Oikos,* **102,** 407–412.

Francey, R. J., and Coauthors, 1999: A 1000-year high precision record of $\delta^{13}C$ in atmospheric CO_2. *Tellus,* **51B,** 170–193.

Gagen, M., D. McCarroll, N. J. Loader, I. Robertson, R. Jalkanen, and K. J. Anchukaitis, 2007: Exorcising the 'segment length curse': Summer temperature reconstruction since AD 1640 using non-detrended stable carbon isotope ratios from pine trees in northern Finland. *Holocene,* **17,** 435–446.

Gaudinski, J. B., and Coauthors, 2005: Comparative analysis of cellulose preparation techniques for use with ^{13}C, ^{14}C, and ^{18}O isotopic measurements. *Anal. Chem.,* **77,** 7212–7224.

Graham, E. A., S. S. Mulkey, K. Kitajima, N. G. Phillips, and S. J. Wright, 2003: Cloud cover limits net CO_2 uptake and growth of a rainforest tree during tropical rainy seasons. *Proc. Natl. Acad. Sci. USA,* **100,** 572.

Grinsted, A., J. C. Moore, and S. Jevrejeva, 2004: Application of the cross wavelet transform and wavelet coherence to geophysical time series. *Nonlinear Processes Geophys.,* **11,** 561–566.

Haylock, M. R., and Coauthors, 2006: Trends in total and extreme South American rainfall in 1960–2000 and links with sea surface temperature. *J. Climate,* **19,** 1490–1512.

Hoffmann, G., and Coauthors, 2003: Coherent isotope history of Andean ice cores over the last century. *Geophys. Res. Lett.,* **30,** 1179, doi:10.1029/2002GL014870.

Holmes, R. L., 1983: Computer-assisted quality control in tree-ring dating and measurement. *Tree-Ring Bull.,* No. 43, 69–78.

Huete, A. R., and Coauthors, 2006: Amazon rainforests green-up with sunlight in dry season. *Geophys. Res. Lett.,* **33,** L06405, doi:10.1029/2005GL025583.

IAEA/WMO, cited 2004: Global Network of Isotopes in Precipitation. GNIP Database. [Available online at http://www-naweb.iaea.org/napc/ih/IHS_resources_gnip.html.]

Jones, P. D., and M. E. Mann, 2004: Climate over past millennia. *Rev. Geophys.,* **42,** RG2002, doi:10.1029/2003RG000143.

Keeling, C. D., 1961: A mechanism for cyclic enrichment of carbon-12 by terrestrial plants. *Geochim. Cosmochim. Acta,* **24,** 299–313.

Li, Z.-H., S. W. Leavitt, C. I. Mora, and R.-M. Liu, 2005: Influence of earlywood–latewood size and isotope differences on long-term tree-ring $\delta^{13}C$ trends. *Chem. Geol.,* **216,** 191–201.

Lyon, B., 2004: The strength of El Niño and the spatial extent of tropical drought. *Geophys. Res. Lett.,* **31,** L21204, doi:10.1029/2004GL020901.

Majoube, M., 1971: Fractionnement en oxygéne-18 et en deutérium entre l'eau et sa vapeur. *J. Chim. Phys.,* **58,** 1423–1436.

Malhi, Y., and J. Wright, 2004: Spatial patterns and recent trends in the climate of tropical rainforest regions. *Philos. Trans. Roy. Soc. London,* **359B,** 311–329.

Manning, M. R., and W. H. Melhuish, 1994: Atmospheric δ^{14}C record from Wellington. *Trends '93: A Compendium of Data on Global Change,* T. A. Boden et al., Eds., Oak Ridge National Laboratory Carbon Dioxide Information Analysis Center Publication ORNL/CDIA C65, 193–202.

Marengo, J. A., and Coauthors, 2008: The drought of Amazonia in 2005. *J. Climate,* **21,** 495–516.

Morales, M. S., R. Villalba, H. R. Grau, and L. Paolini, 2004: Rainfall-controlled tree growth in high-elevation subtropical treelines. *Ecology,* **85,** 3080–3089.

Münnich, M., and J. D. Neelin, 2005: Seasonal influence of ENSO on the Atlantic ITCZ and equatorial South America. *Geophys. Res. Lett.,* **32,** L21709, doi:10.1029/2005GL023900.

Murphy, P. G., and A. E. Lugo, 1986: Ecology of tropical dry forest. *Annu. Rev. Ecol. Syst.,* **17,** 67–88.

Nepstad, D. C., and Coauthors, 1994: The role of deep roots in the hydrological and carbon cycles of Amazonian forests and pastures. *Nature,* **372,** 666–669.

——, and Coauthors, 2002: The effects of partial throughfall exclusion on canopy processes, aboveground production, and biogeochemistry of an Amazon forest. *J. Geophys. Res.,* **107,** 8085, doi:10.1029/2001JD000360.

Nychka, D., 2007: Fields: Tools for spatial data. R package, version 3.5. [Available online at http://www.image.ucar.edu/GSP/Software/Fields/.]

Nydal, R., and K. Lövseth, 1983: Tracing bomb ^{14}C in the atmosphere 1962–1980. *J. Geophys. Res.,* **88,** 3621–3642.

Oliveira, R. S., T. E. Dawson, S. S. Burgess, and D. C. Nepstad, 2005: Hydraulic redistribution in three Amazonian trees. *Oecologia,* **145,** 354–363.

Poussart, P. F., and D. P. Schrag, 2005: Seasonally resolved stable isotope chronologies from northern Thailand deciduous trees. *Earth Planet. Sci. Lett.,* **235,** 752–765.

——, M. N. Evans, and D. P. Schrag, 2004: Resolving seasonality in tropical trees: Multi-decade, high-resolution oxygen and carbon isotope records from Indonesia and Thailand. *Earth Planet. Sci. Lett.,* **218,** 301–316.

Ramesh, R., S. K. Bhattacharya, and G. B. Pant, 1989: Climatic significance of $_{\delta}$D variations in a tropical tree species from India. *Nature,* **337,** 149–150.

Roden, J. S., G. Lin, and J. R. Ehleringer, 2000: A mechanistic model for interpretation of hydrogen and oxygen isotope ratios in tree-ring cellulose. *Geochim. Cosmochim. Acta,* **64,** 21–35.

Rozanski, K., L. Araguas-Araguas, and R. Gonfiantini, 1993: Isotopic patterns in modern global precipitation. *Climate Change in Continental Isotopic Records, Geophys. Monogr.,* Vol. 78, 1–36.

Sachs, J. P., D. Sachse, R. H. Smittenberg, Z. Zhang, D. S. Battisti, and S. Golubic, 2009: Southward movement of the Pacific intertropical convergence zone AD 1400–1850. *Nat. Geosci.,* **2,** 519–525.

Salati, E., and P. B. Vose, 1984: Amazon basin: A system in equilibrium. *Science,* **225,** 129–138.

Saleska, S. R., and Coauthors, 2003: Carbon in Amazon forests: Unexpected seasonal fluxes and disturbance-induced losses. *Science,* **302,** 1554–1557.

Solíz, C., R. Villalba, J. Argollo, M. S. Morales, D. A. Christie, J. Moya, and J. Pacajes, 2009: Spatio-temporal variations in *Polylepis tarapacana* radial growth across the Bolivian Altiplano during the 20th century. *Palaeogeogr. Palaeoclimatol. Palaeoecol.,* **281,** 296–308.

Sternberg, L. S. L. O., and M. J. Deniro, 1983: Biogeochemical implications of the isotopic equilibrium fractionation factor between the oxygen atoms of acetone and water. *Geochim. Cosmochim. Acta,* **47,** 2271–2274.

Terborgh, J., C. Flores, N. P. Mueller, and L. Davenport, 1997: Estimating the ages of successional stands of tropical trees from growth increments. *J. Trop. Ecol.,* **13,** 833–856.

Thompson, L. G., E. Mosley-Thompson, W. Dansgaard, and P. M. Grootes, 1986: The Little Ice Age as recorded in the stratigraphy of the Tropical Quelccaya Ice Cap. *Science,* **234,** 361–364.

Trenberth, K. E., 1997: The definition of El Niño. *Bull. Amer. Meteor. Soc.,* **78,** 2771–2777.

——, and Coauthors, 2007: Observations: Surface and atmospheric climate change. *Climate Change 2007: The Physical Science Basis,* S. Solomon et al., Eds., Cambridge University Press, 235–336.

Treydte, K. S., G. H. Schleser, G. Helle, D. C. Frank, M. Winiger, G. H. Haug, and J. Esper, 2006: The twentieth century was the wettest period in northern Pakistan over the past millennium. *Nature,* **440,** 1179–1182.

Tudhope, A. W., and Coauthors, 2001: Variability in the El Niño-Southern Oscillation through a glacial-interglacial cycle. *Science,* **291,** 1511–1517.

Urban, F. E., J. E. Cole, and J. T. Overpeck, 2000: Influence of mean climate change on climate variability from a 155-year tropical Pacific coral record. *Nature,* **407,** 989–993.

Villalba, R., R. L. Holmes, and J. A. Boninsegna, 1992: Spatial patterns of climate and tree growth variations in subtropical northwestern Argentina. *J. Biogeogr.,* **19,** 631–649.

——, E. R. Cook, G. C. Jacoby, R. D. D'Arrigo, T. T. Veblen, and P. D. Jones, 1998: Tree-ring based reconstructions of northern Patagonia precipitation since AD 1600. *Holocene,* **8,** 659.

Vuille, M., and M. Werner, 2005: Stable isotopes in precipitation recording South American summer monsoon and ENSO variability: Observations and model results. *Climate Dyn.,* **25,** 401–413.

——, R. S. Bradley, R. Healy, M. Werner, D. R. Hardy, L. G. Thompson, and F. Keimig, 2003: Modeling δ^{18}O in precipitation over the tropical Americas: 2. Simulation of the stable isotope signal in Andean ice cores. *J. Geophys. Res.,* **108,** 4175, doi:10.1029/2001JD002039.

Worbes, M., 1999: Annual growth rings, rainfall-dependent growth and long-term growth patterns of tropical trees from the Caparo Forest Reserve in Venezuela. *J. Ecol.,* **87,** 391–403.

Zhang, X., F. W. Zwiers, G. C. Hegerl, F. H. Lambert, N. P. Gillett, S. Solomon, P. A. Stott, and T. Nozawa, 2007: Detection of human influence on twentieth-century precipitation trends. *Nature,* **448,** 461–465.